March 2015

Hydrogeological control on spatial patterns of groundwater seepage in peatlands

Danielle K. Hare
University of Massachusetts Amherst

Hydrogeological control on spatial patterns of groundwater seepage in peatlands

A Thesis Presented

By

DANIELLE K. HARE

Submitted to the Graduate School of the
University of Massachusetts Amherst in partial fulfillment
of the requirements for the degree of

MASTER OF SCIENCE

February 2015

Department of Geosciences

Hydrogeological control on spatial patterns of groundwater seepage in peatlands

A Thesis Presented

By

DANIELLE K. HARE

Approved as to style and content by:

_____
David. F. Boutt, Chair

_____
Christine Hatch, Member

_____
William Clement, Member

_____
Julie Brigham-Grette, Department Head
Department of Geosciences

DEDICATION

To my Family- for their patience, encouragement and love.

ACKNOWLEDGEMENTS

ABSTRACT

HYDROGEOLOGICAL CONTROL ON SPATIAL PATTERNS OF GROUNDWATER

SEEPAGE IN PEATLANDS

FEBRUARY 2015

DANIELLE HARE, B.S., SYRACUSE UNIVERSITY

M.S., UNIVERSITY OF MASSACHUSETTS AMHERST

Directed by: Dr. David F. Boutt

Groundwater seepage to surface water is an important process to peatland ecosystems; however, the processes controlling seepage zone distribution and magnitude are not well understood. This lack of process-based understanding makes degraded peatland ecosystems difficult to restore and problematic for resource managers developing a sustainable design. Degraded peatlands, particularly abandoned cranberry farms, often have drainage ditches, applied surface sand, and decreased stream sinuosity to artificially lower the water table and support agriculture. These modifications disconnect the surface and groundwater continuum, which decreases thermal buffering of surface water significantly. The combination of a decreased influx of thermally buffered groundwater, a naturally low surface gradient, minimal canopy, and strong solar input causes surface water temperature extremes that degrade ecosystem health. Through strategically incorporating the natural processes to restore groundwater discharge to restored surface streams, surface water temperature extremes will be buffered promoting a healthy, resilient wetland ecosystem. Therefore, it is critical to understand the spatial

hydrogeologic constraints that induce groundwater seepage. Here we examine the spatial relationship between surficial groundwater seepage and the subsurface hydrogeologic structure within a mineraltrophic peatland environment. We use multiple field methods to develop a process-based conceptual model of the ground water seepage development at the site; these methods include geophysical, thermal, and isotopic techniques. The results indicate that there are two distinct forms of groundwater discharge to the peatland platform: diffuse lower-flux marginal seepage and discrete higher-flux interior seepage. Both types of groundwater discharge develop through interactions with subsurface peatland basin structure, specifically when the basin slope is perpendicular to the regional groundwater gradient. These observations also allow insight into the formation of the groundwater discharge through time. The strong correlation between the subsurface basin structure and surficial groundwater expression will allow resource managers to more efficiently locate groundwater seepage on large, complex sites, and develop comprehensive management and restoration strategies for these critical ecosystems.

TABLE OF CONTENTS

LIST OF TABLES

Table   Page

CHAPTER 1

INTRODUCTION

Hydrologic processes have been recognized as the dominant control on peatland development (*Clymo*, 1984; *Belyea and Clymo*, 2001; *Larsen et al.*, 2007; *Ise et al.*, 2008; *Rennermalm et al.*, 2010), peatland vegetation patterning (*Kettridge et al.*, 2008) and the decomposition degree of peat (*Boelter*, 1969; *Chason and Siegel*, 1986). Of these hydrologic processes, groundwater seepage is one of the most important physical controls on the surficial ecosystem stability (*Siegel et al.*, 1995; *Watters and Stanley*, 2007), despite the poor understanding of the underlying physical hydrogeologic framework governing the seepage distribution. Preferential flow paths, hydraulic conductivity anisotropy, and geologic heterogeneities may control the surface expression of seepage zones (*Chason and Siegel*, 1986; *Drexler et al.*, 1999; *Smart et al.*, 2012), but these features have been difficult to constrain due to the spatial resolution of traditional localized groundwater wetland methods (wells, boreholes, surface point measurements, etc.).

Peatland-scale patterns and structures, on the order of km^2, are typically difficult to identify and interpret due to strong heterogeneous and isotropic tendencies. However, the use of multiple tracer methods and geophysical data offer the potential to conceptualize large scale processes that may have been missed or misinterpreted with typical localized hydrologic investigations (*Lowry et al.*, 2007, 2009; *Kettridge et al.*, 2008; *Briggs et al.*, 2012). As peat accumulates, the organic matter is composed of changing surficial vegetation that has experienced various environmental conditions.

These cause changes in the peat composition, which impact decomposition with depth; also, macropores have been shown to contribute greatly to peatland hydrodynamics and transport (*Holden and Burt*, 2003; *Jones*, 2010). This makes interpreting hydraulic gradients difficult, and invasive equipment installations may modify flow the fragile flow regime. Therefore, at these large, dynamic sites we attempt to analyze large-scale patterns across the entire peatland using noninvasive techniques.

Groundwater discharge to surface aquatic systems provide aquatic species habitat, which is important for ecosystem health (*van Loon et al.*, 2009), as the groundwater temperatures remain relatively constant compared to surface water. Surficial water thermal stability has been a popular research focus in hydro-ecology, as this process is important for aquatic species (e.g. fish) that rely on the low thermal variance groundwater to buffer themselves from heat extremes and regulate their metabolism (*Caissie*, 2006; *Deitchman and Loheide II*, 2012). Temperature also controls chemical processes such as solubility, diffusivity, and reaction rates, which play an immediate role in ecosystem respiration. Ecosystem respiration controls the ecosystem's carbon emission and nutrient retention (*Boulton et al.*, 1998; *Lafleur et al.*, 2005; *Davidson and Janssens*, 2006; *Demars et al.*, 2011), biodiversity (*Parish et al.*, 2008), and overall species health (*Verberk et al.*, 2011). An increase in wetland temperature also has been shown to stimulate methane production (*McKenzie et al.*, 2007). In wetlands groundwater inputs are the dominate source of solute influx and may serve as spatial hotspots for biogeochemical cycling (*Sebestyen and Schneider*, 2001). Upwelling zones also maintain species richness, which has been attributed to an 'edge effect' caused by overlap between

the thermal and chemically stable groundwater ecotone and the higher oxygen environment within the main stream channel (*Brunke and Gonser*, 1997; *Cirkel et al.*, 2010). Therefore, determining the processes that control the spatial patterns, magnitude, and temperature of groundwater seepage is of concern for multi-disciplinary researchers and water resource managers.

Of concern for New England water resource managers are the current cultivated, highly managed cranberry farms within the region. Peatland environments are ideal for cranberry farming as cranberries (*Vaccinium macrocarpon*) prefer acidic, organic-rich soils, and peatlands are usually close to a source of water for flooding that provides frost protection and facilitates harvest (*Garrison and Fitzgerald*, 2005; *DeMoranville*, 2006). Historically, cranberry peatlands are converted natural wetlands (*Garrison and Fitzgerald*, 2005) where through-flow streams are straightened and channels dug to artificially lower the peatland's natural water table (*Price et al.*, 2003). These anthropogenic modifications severely degrade the natural processes within a wetland by creating a discontinuity between surface water and groundwater systems, an interaction that is critical for wetland function.

New England's natural peatland cranberry agriculture has been declining due to an increased efficiency of constructed upland cranberry farms in the north-central states of the USA as well as eastern Canadian provinces. An increasing number of New England natural peatland cranberry operations will stop farming, which will present an opportunity to restore these drained sites to fully functioning peatland ecosystems. These

restorations are important for protecting aquifer water quality and quantity (M.G.L ch.131 §40 (2000)). Cranberry farm/peatland restorations have begun to increase locally; however, managers have voiced concern over the lack of process-based data available for peatland ecosystem development.

We describe the development and spatial distribution of groundwater seepage within a hydrologic landscape as a function of geology, the basin structure and hydraulic properties of the peatland matrix. We focus on understanding the natural processes that promote the hydrologic inputs for aquatic habitat formation and ecosystem stabilization. These results allow restoration design to account for the driving mechanisms that support groundwater seepage with the goal of developing naturally sustainable and self-sufficient ecosystems (e.g. process-based design (*Dahl et al.*, 2007)). Process-based restoration design is an approach that attempts to restore the natural processes that will reverse the predominate cause(s) of degradation at a site (*Beechie et al.*, 2010). Process-based principles are based upon physical laws congruent with natural structures (*Cardenas and Zlotnik*, 2003), and are utilized to encourage natural processes in managed or restored land (*Beechie et al.*, 2010).

We seek to determine the subsurface mechanisms behind the formation and persistence of surficial groundwater seepage locations in a groundwater-fed, temperate peatland. We deploy multiple methods including: fiber-optic distributed temperature sensing; infrared imagery; temperature profiles; stable water isotope methods; and ground penetrating radar surveys, to identify the location and source of groundwater inputs to the

4

peatland surface. We hypothesize that the distribution of groundwater discharge locations and their magnitude are governed by stochastic processes, but form from a predictable process generated by consistent changes in subsurface pressure gradients. The goals of this study are to: (1) identify groundwater discharge locations and their hydrogeologic controls, (2) determine temperature dynamics of the groundwater discharge locations, (3) identify groundwater sources of these contributing flow paths, and (4) evaluate the development of these seepage patterns over time.

BACKGROUND

2.1 Peatland Hydrology

Peatlands are generated through the accumulation of organic matter, which occurs when vegetation accumulation exceeds vegetation decomposition, typically in anoxic conditions (*Clymo*, 1984; *Parish et al.*, 2008). The rate at which organic matter decomposes is a function of the oxygen exposure time and vegetation type because the rate of decomposition varies between species. Plant species are sensitive to hydrologic and climatic changes, and can vary spatially as well as temporally across the site. These variations in the degree of decomposition causing peat hydraulic conductivity to be temporally dynamic, heterogeneous and strongly anisotropic (*Boelter*, 1968, 1969; *Grover and Baldock*, 2013). As hydrology and climate control vegetation type (*Robinson et al.*, 2008), a complex feedback for the accumulation/decomposition of the peat organic matter matrix develops and varies as climatic changes, site hydrology varies, and with differences in vegetation species (*Clymo*, 1984; *Belyea and Clymo*, 2001).

This complex feedback can be observed as a stark difference in hydraulic properties with depth. The upper most layer of peat (~10-50 cm depth) is the acrotelm, and generally exhibits a high hydraulic conductivity as the organic matter is relatively young, but does experience a high rate of decomposition as it is typically above the water table and is decomposing aerobically. The anaerobic catotelm develops below the acrotelm (>50 cm depth) -- typically below the water table. As the organic matter

continues to decompose, the matrix becomes more compact, causing the permeability to decrease (*Clymo*, 1984). However, it is observed that there is little correlation between peat permeability and depth (*Chason and Siegel*, 1986) due to the fact that the rate decomposition is controlled by changes in vegetation litter, temperature and water level (*Ise et al.*, 2008), and is not a function of time.

Large-scale peat depressions extend well beneath the water table into the subsurface, disrupting local and regional flow paths (*Winter and Labaugh*, 2003). These depression modify flow paths around a peat body and can create points of focused hydraulic pressure below the peat surface (*Slater and Reeve*, 2002; *Lowry et al.*, 2009). The water table within a peatland is complex in regards to the surrounding aquifer, and can be important aquifer sources or sinks. A peatland that is a source of recharge for the underlying aquifer is an ombrotrophic or bog peatland. These environments create localized groundwater mounds caused by the low hydraulic conductivity peat compared to the surrounding aquifer materials. These environments are have low nutrients as nutrient-poor precipitation is the predominant source of water. A mineraltrophic or fen peatland is a discharge zone for the underlying aquifer and is typically nutrient-rich. Flow reversals are common within peatland environments, switching between ombrotrophic and mineraltrophic type of peatland (*Devito et al.*, 1997; *Reeve et al.*, 2000; *Fraser et al.*, 2001), but unlikely at our site due to the strong regional flow gradients maintaining a constant source gradient to the site. Localized flow cells have also been observed in bog-fen complexes that interact with the regional groundwater systems promoting unique flow paths beneath these types of peatlands (*Siegel et al.*, 1995; *Reeve et al.*, 2000).

Pore water movement was previously thought to be negligible in the low hydraulic conductivity catotelm (10^{-5} – 10^{-8} m s^{-1}) (*Chason and Siegel*, 1986; *Reeve et al.*, 2000). However, numerous studies have refuted this assumption and claim that both lateral flow and vertical flow exist within the catotelm depending on the contrasting hydraulic conductivity beneath catotelm (e.g. *Siegel et al.*, 1995; *Glaser et al.*, 2004). If the underlying sediment has a lower permeability, then lateral flow will be expected, and if the permeability is higher, vertical flow is expected (*Reeve et al.*, 2000). The induced flow through peatland pores is believed to be minimal, but still significant for surface water processes. Studies show that macro-scale structures cause increases in hydraulic conductivity may be important in transport from vertical flow, and provides an additional mechanism to explain the connection between pore water chemistry and the underlying groundwater systems (*Siegel et al.*, 1995).

Groundwater flow in peatlands has been described as focused macropore flow (preferential flow paths) rather than diffuse, uniform flow through the peat matrix (*Baird*, 1997; *Beckwith et al.*, 2003; *Holden*, 2004; *Wallage and Holden*, 2011). The specific mechanics controlling the development and the resulting spatial distribution of these macropore flow paths are unknown, having been described as "large branch-like networks" (*Holden*, 2004; *Holden et al.*, 2012; *Smart et al.*, 2012). Authors have speculated that the spatial development of these discrete discharge locations is due to vegetation deposition and rooting, burrowing hollows (*Baird*, 1997), wetland inundation patterns, and/or tearing of peat (*Smart et al.*, 2012). Attempts to determine the spatial

extent of these discrete internal flow paths have been explored in previous work, but the success has been limited, and the mechanics not well understood.

Baird (1997) first quantified the presence of near-surface macropore flow into a groundwater-fed peatland environment and its importance in fluid and solute flux. *Beckwith et al.* (2003) demonstrated through numerical modelling that fine scale variations within the peat substrate affect flow dynamics, emphasizing flow through areas of inherent weakness in the peat matrix rather than patterns of diffuse, uniform flow. *Holden* (2005) establishes that macropores, or "pipes" are critical in peatland runoff and infiltration dynamics, and are also important in carbon export. The spatial distribution of macropores was quantified through visual, geophysical, and geochemical techniques (*Worrall et al.*, 2010; *Wallage and Holden*, 2011; *Smart et al.*, 2012; *Cunliffe et al.*, 2013); however these methods were installed too localized to characterize the macropore network on a site scale. *Lowry et al.* (2009) theorized that at locations where there was dramatic steepening in the peat basin slope, and where this steepening was orientated perpendicular to the regional groundwater gradient, large groundwater seepage formed. Using ground penetrating radar (GPR), aerial photography and 3-D groundwater flow modeling, *Lowry et al. (*2009*)* hypothesized that seepage occurs at these locations because the peat thickness increases rapidly thinning the aquifer beneath. This causes a dramatic decrease in the hydraulic conductivity forcing the hydraulic head gradient to steepen inducing upward flux, and therefore groundwater seepage. While *Lowry et al.,* (2009) provided both field and modeling results they state that further field work is necessary to provide background field observations of this phenomena. *Rossi et al.*

(2012) supports this theory in a peatland with underlying esker forms. *Comas et al.* (2011) observed a relation between water pooling and a thinning of peat through geophysical data and remote sensing; however the authors state the importance of developing a comprehensive understanding of the underlying hydrologic mechanisms.

Peatland groundwater seepage research has focused on macropore flows, and has described this process as an important source of influx of groundwater to peatland systems, but this may be a bias due to localized sampling techniques and method resolution. While macropores flows exist, diffuse inflow and macropore/discrete flows may also be important groundwater contributors, as spatially diffuse inflows may also be prevalent across the peatland surface. Therefore, it is important to analyze both types of groundwater input and the separate hydrodynamics that control these unique surface fluxes using field observations.

2.2 Site Description

Tidmarsh Farms was a cultivated peatland (2.5 km^2) since the early 1900s that ceased cranberry farming operations in 2010. This site is a kettle hole peatland complex located in Manomet, Plymouth County, Massachusetts. Tidmarsh Farms drains the 5 km^2 Beaver Dam Watershed, yet is the discharge location of the 360 km^2 Plymouth-Carver-Kingston-Duxbury groundwater aquifer. Surface water enters the site from four surface water bodies south of the site (Fresh Pond, Little Island Pond, the Arm Wetland, and Beaver Dam Pond (which was drained in 2011)), and drains northward into Beaver Dam Brook, an approximately 2 kilometers reach, before discharging in Bartlett Pond and then directly into Plymouth Bay (Figure 1).

10

2.2.1 Farming Modifications

Beaver Dam Pond was previously dammed at its entry onto the farm site to create a reservoir. This provided the ability to flood the property for farming purposes. The flashboards in the dam were removed in the fall of 2010, and the peatland farm site has been allowed to return to a natural state without any new anthropogenic influence.

Sand was applied to the site since the early 1900s, and at our studied site 0.3-1.5 meters of sand overlies the peat surface. This applied sand was mined from an onsite glacial outwash outcrop. At Tidmarsh Farms, parallel drainage ditches were dug approximately every 35 meters throughout the entire site, and are approximately 1 meter wide and 0.5 meter deep. The west peat cells have drainage ditches oriented east-west, and in the east cells most drainage ditches are oriented north-south (exceptions within Cell 7).

2.2.2 Hydrogeology

The Plymouth-Carver-Kingston-Duxbury (PCKD) regional aquifer system is the second largest aquifer in Massachusetts and is an unconfined aquifer comprised mostly of unconsolidated glacial deposits ranging from clay to gravel sized clasts (*Masterson*, 2009; *Newby et al.*, 2009). This aquifer provides water for four counties, and hosts abundant cranberry agriculture and wetland ecosystems. Contours of the regional water table elevation show a strong regional northeast gradient at the Tidmarsh Farms site, as shown by the flow lines in Figure 1. We confirm the northeast groundwater flow

direction with onsite groundwater well measurements. These flow lines also confirm that this site is a discharge location for the larger, regional aquifer (*Hansen and Lapham*, 1992; *Masterson*, 2009), which is important in understanding the peatland developmental history.

Ocean bounds the regional aquifer on both the east and south. The northern and western boundaries are the Green Harbor River and the Winnetuxet River respectively (Figure 1). The primary source of recharge is precipitation, and the aquifer responds quickly as the recharge deposits are high hydraulic conductivity outwash plain deposits: the Wareham and Carver Pitted Plains deposits (*Masterson*, 2009). This fast response to precipitation makes this regional aquifer sensitive to climatic changes (*Shuman et al.*, 2001; *Newby et al.*, 2009). Newby et al. (2000, 2009) analyzed paleolimnologicial water level fluctuations within the regional aquifer, determining the regional aquifer's water table was quite variable subsequent to the retreat of the Laurentide ice sheet (~16 ka). Notably during the Younger Dryas (~11 ka) the water levels in the PCKD aquifer were very low compared with present day, and were very slow to recover, as these dry conditions persisted until ~5 ka (*Newby et al.*, 2000). Topographic changes caused by isostatic rebound and sea level rise could also attribute to the water table elevation changes by changing base level (*Oakley and Boothroyd*, 2012). Historical water levels are important to understanding the development of surface water-groundwater interactions within peatlands as water level determines hydraulic gradients on and around the site, and groundwater driven periods of low-stands/shallow lakes promote peat accumulation within regional kettle ponds.

2.3 Peatland Development

At Tidmarsh Farms as the Laurentide ice sheet retreated from the Southern coast of Massachusetts. There were a complex series of small scale ice lobe advances and retreats generating the sediment distribution patterns in this area (*Koteff and Pessl*, 1981; *Larson*, 1982). These evolved into outwash plains and recessional moraines, which were subsequently flooded by ice-margin lakes (*Larson*, 1982). As a result, glacial outwash deposits, kame deltas, ground moraines, and ice collapse features and deformation surround Tidmarsh Farms (*Larson*, 1982; *Stone et al.*, 2011). The ice collapse features and kettle holes are typical of environments proximal to ice contact zones. There is extensive evidence of these features throughout the surrounding region (Figure 1). Kettle holes are depressions in the land surface that are caused when the glacial ice retreats and large pieces of ice calve off the retreating ice lobe. The ice remains in place and outwash sediments accumulate around it. Once the ice melts an accommodation space is left, and if the depression intercepts with the water table this space becomes a pond. Kettle holes/ponds are common in New England, and many have developed into peatlands.

Peatlands can form through two different modes: paludification (i.e. terrestrial sites), or terrestrialization (i.e. infill of lake basins). Paludification is typical of boreal, low land environments, whereas terrestrialization requires the presence of shallow lakes, such as the kettle ponds within outwash plains, and is more typically found within temperate environments (*Buffam et al.*, 2010). This distinction is important to understand peatland hydrodynamics. The underlying geomorphology in a paludification peatland is relatively constant, with no strong changes in depth, whereas peatlands formed through terrestrialization have a complex basin structure. Due to the presence of nearby lakes, the

13

Figure 1: Regional map of the study site. Regional northeast groundwater flow lines indicate that the groundwater divides are much larger than the watershed boundaries, and these wetlands are discharging from a greater volume than the watershed receives. Three bodies of water drain into Tidmarsh Farms wetland: Fresh Pond, the Arm, and Beaver Dam Pond/headwaters. Surface water drains northward, and becomes the singular Beaver Dam Brook on site before discharging into Plymouth Bay.

temperate environment, and kettle hole structure, we assume that our peatland site formed through the process of terrestrialization.

Originally, to accumulate peat in a lake/pond setting, organic matter must have limited oxygen exposure; therefore, an anoxic aquatic environment is required to prevent the decomposition of wetland vegetation. Carbon burial rates, inversely proportional to oxygen exposure time, have shown to increase in lakes that are deep relative to their surface area (*Ferland et al.*, 2014). This basin structure is similar to many small glacial kettle ponds with deep irregular shapes due to the ice collapse formation. The irregular geometry also may modify lake turnover. This type of environment may be more likely to induce the anoxic conditions necessary to promote peat accumulation.

Post-glacial water table levels are important to understanding sediment/peat accumulation, the degree of decomposition of organic matter, sediment infill and changes in vegetation that can be expected within the peat matrix. Temporal dynamics of the water table position induce much of the spatial variability in hydraulic conductivity (*Clymo*, 1984). This is most notable in the difference between the catotelm and the acrotelm. The rate at which the peat thickness increases is a fine balance between the continual submersion of organic matter and maintaining shallow waters. An anoxic sub-aqueous environment slows decay of the organic matter allowing the peat to accumulate (*Clymo*, 1984; *Belyea and Clymo*, 2001). *Belyea and Clymo* (2001) indicate that if the matrix remains constant, seepage varies with the lateral peat growth will determine the shape of the peatland. Overall, these complex interactions between water table, climate,

and vegetation define the mechanisms for growth of peatlands and the hydrologic properties of the peat matrix. This emphasizes the importance of understanding the past development of peat to constrain present day peatland hydrodynamics.

2.4 Peatland Restoration

Peatlands provide a unique environment for ecosystem services including carbon storage, nutrient retention, and water storage. Widespread drainage of peatlands has caused catastrophic degradation to the hydrological and ecological services these environments provide. Within the United Kingdom there has been significant movement to return of the natural water table level to these wetlands by filling in drainage ditches; however there are disagreements as to the cost-benefits of these restoration designs (*Grand-Clement et al.*, 2013). As the length of recovery is exceeds to the recovered monitoring data, linking the success to these mitigation techniques is inconclusive. In addition, natural peatland processes have also proven difficult to constrain due to the localized, dynamic nature of the substrate inhibiting process-based design. This incomplete process understanding has limited successful restoration projects, particularly within the surface water temperature health. Our study emphasizes the importance of understanding these underlying physical controls on the hydrological process that drive and promote healthy, thermally-buffered ecosystems, and desirable ecosystem services. Our results will aid water resource managers in developing a process-based design based on large-scale hydrological process with little site invasion.

Beyond establishing the dominant controls underlying surficial process, this study provides background pre-restoration data for a comprehensive comparison before and

after the restorative modifications. This is much needed data as little pre-restoration baseline data exist making evaluation difficult, and without baseline data a critical reflection on the design practices implemented cannot occur. Tidmarsh Farms has begun a long-term ecological monitoring plan that will better constrain the effects of the restoration and develop a better understanding of the natural process that control peatland dynamics.

CHAPTER 3

METHODS

Seepage patterns within peatlands have been difficult to constrain due to large site areas and complex, dynamic materials. In addition, peatlands may not adhere to the laws of steady-state Darcian flow because peatlands exhibit dynamic hydraulic conductivity as well as the influences of multiple phases and dominance of macropore flow paths (*Rycroft et al.*, 1975). These dynamics has made it difficult to interpret peatland hydrodynamics using traditional invasive methods that disturb the peat. While non-Darcian flow is inconclusive, it has been observed that free-phase gas accumulation (*Kellner et al.*, 2004; *Reeve et al.*, 2006; *McKenzie et al.*, 2007; *Parsekian et al.*, 2011) as well as the presence of preferential flow paths (*Holden*, 2004; *Worrall et al.*, 2010; *Wallage and Holden*, 2011; *Hill*, 2012; *Smart et al.*, 2012; *Cunliffe et al.*, 2013; *Vandenbohede et al.*, 2014) both greatly influence the peatland flow regime.

We use multiple methods to combat this unique environment that are novel for peatlands. Our research builds on hypotheses presented in Lowry et al. (*2009*), and examines how groundwater seepage is spatially distributed within a fen peatland. We use a geophysical technique to evaluate the subsurface structure of the peatland basin, multiple temperature methods to locate surficial groundwater seepage, and stable water isotopes to describe dominant up gradient sources supplying the seepage.

3.1. Resolving Subsurface Structure

Wetland sites can be laterally expansive and exhibit dynamic hydrogeologic characteristics, which makes localized hydrogeologic techniques, such as groundwater wells and boreholes, difficult to implement on a representative scale and interpret appropriately (*Kettridge et al.*, 2008). Near-surface geophysical techniques permit collection of noninvasive, high resolution data sets that can cover large areas efficiently, which makes these methods more ideal for wetland environments (*Fisher et al.*, 1992; *Knight*, 2001; *Leopold and Volkel*, 2003; *Comas et al.*, 2005). Ground penetrating radar (GPR) has been successfully used to characterize peatlands' physical structure and stratigraphy due to the distinct discontinuity between peat and the underling aquifer geophysical properties (e.g. water content) (e.g. *Slater and Reeve*, 2002; *Holden*, 2004; *Comas et al.*, 2005; *Lowry et al.*, 2009). GPR has also been successfully used to characterize subsurface hydrologic patterns to compare to surficial ecological patterns (*Kettridge et al.*, 2008). GPR transmit electromagnetic (EM) waves through the subsurface then records the time and amplitude of the returning signal (reflection) to image heterogeneities in the electromagnetic characteristics between subsurface materials (*Knight*, 2001; *Lowry et al.*, 2009). The dielectric permittivity controls the velocity of EM signal, and is primarily a function of a material's moisture content (*Topp et al.*, 1980). As peat has a high porosity (n= 0.4-0.8) in comparison to unconsolidated glacial aquifers that typically underlie kettle peatlands (n=~0.3). This large difference in water content typically allows for better resolution of the boundary between these two materials. We used common-offset reflection profiling to acquire GPR data with both 100 MHz and 50 MHz antennas, and a transmitter-receiver separation at 1 meter and 2 meters respectively;
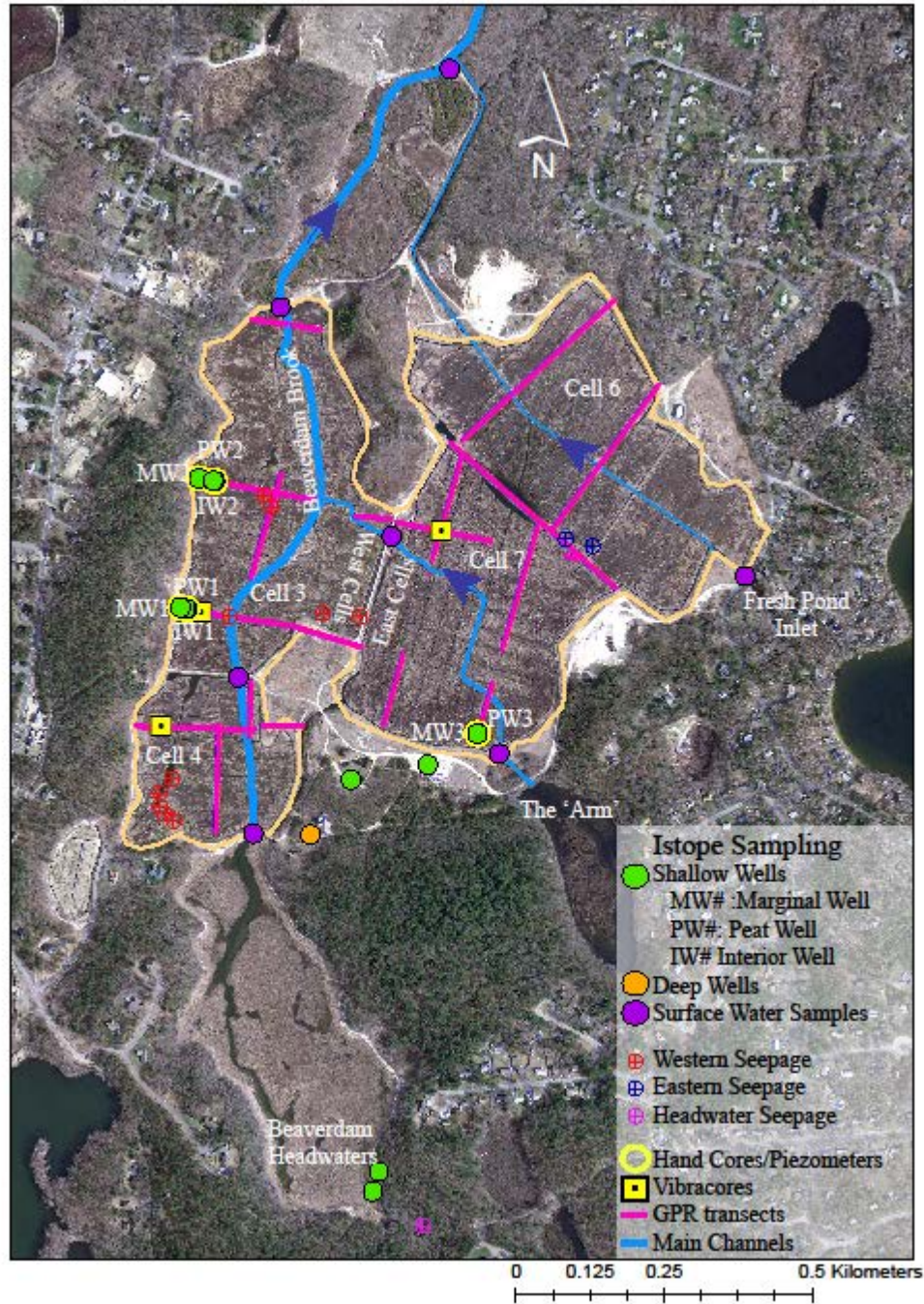
Figure 2: Tidmarsh Farms study site. All sampling locations for stable water isotopes, geophysical surveys, and peat cores. All surface water flows north towards Plymouth Bay. Large stream channels are indicated by the blue lines and flow direction by the arrow heads.

however, only the 100 MHz data was used to generate the interpolations of peat thickness, as they provided better resolution of the peat/sand interface. Nineteen surveys were acquired at the site; all surveys were completed with 0.3 meter trace spacing and ranged from 100 meters to 1000 meters in total length (Figure 2 & 3).

The data were processed with RadExplorer Software from MALA GeoScience to enhance detection of the basal peat-sand aquifer interface. For processing we used a 150 MHz high-cut filter to remove the high frequency noise, and then a 100 ns automatic gain control to compensate for signal loss with depth equalizing the amplitude strength within each trace. The peat-sand interface was then identified in each of the radargrams visually. Any traces that did not produce strong peat- sand reflections are not used in the analysis.

Eight peat cores were collected to constrain the EM signal velocity through the peat and describe the peat's structure with depth (Figure 2). Five peat cores were recovered through multiple collections from each borehole with a 1 meter Russian Peat Core, and were described in the field. Four were collected from the western peat cells, and one on the east peat cells. Three vibracores were also recovered and were visually analyzed. One core is from the east cells, and two from the west cells. The length of the peat in each of these cores were compared to the two-way travel time depth imaged from the radargram reflection from the same location. From these comparisons we were able to calculate an average EM velocity of 0.036 m/ns through the peat. The degree of peat decomposition and porosity varied greatly with depth, but for simplicity, we use this average velocity for the entire thickness and do not separate changes in peat layers. EM

velocity is also expected to change spatially over the site so a single value for EM velocity is expected to not be consistent both laterally. However, due to the similar velocity measured in all the cores, this constant velocity is an appropriate assumption for calculating depth to peat from two-way travel time. This value is also consistent with previous GPR peatland research (0.033-0.039 m/ns) (*Lowry et al.*, 2009). Two-way travel time was converted to meters for all the transects with the calculated EM velocity of 0.036 m/ns and the selected basal peat/ aquifer sand interface.

From the RadExplorer processor, we are able to export the depths for each trace recovered. Then, as all the individual GPR transects were georeferenced as line end points, we linearly interpolate each transect into the number of individual traces recovered to create a georeferenced point for each GPR trace. Through ArcGIS software, we merged the exported depth data to the generated spatial points to create a shape file with peat thic kness at each point included.

To understand the relationship between groundwater seepage and subsurface peat structure, a 3D interpolation of the peat basin shape was created. We generated the peat thickness interpolation using all the EM transect data and ArcGIS spatial analysis toolbox's kriging tool. This enabled us to develop a subsurface characterization of our entire site (Figure 3). Within the kriging tool, anisotropic constraints were used to construct the interpolation to overcome the inconsistency of spacing between GPR transects and station spacing. The anisotropic constraint was created by manually fitting

the model variogram to the raw data variogram (details included in the supplemental materials). The result created is a surface grid of peat thickness for the entire site.

We hypothesize that groundwater seepage is caused at dramatic changes in slope at the basal peat-sand aquifer interface. To test this, we took the 2nd derivative of the maximum slope direction from the generated peat thickness surface grid and developed a profile curvature raster that isolates the local variations in basal peat slope change. The areas of the highest curvature are identified and used this metric as the indicator of strong basal peat slope changes within the interior/center of our peatland site (Figure 3).

3.2. Locating Groundwater Seepage Using Temperature

Groundwater seeps often have distinct thermal, isotopic and geochemical signatures that are a function of subsurface flow paths and water sources. Parameters that are generally more consistent in groundwater than surface waters over time. Therefore, we use these signatures as groundwater tracers; recognizing that the usefulness of each depends on the local groundwater and degree of contrast with surface water. At our site, we use heat signatures to distinguish locations of groundwater inflow in both the summer and winter, and the stable water isotopic signature to evaluate the original source, which we discuss in the next section.

Heat is a naturally occurring, abundant tracer that often contrasts between water sources, which makes heat useful for identifying surface water-groundwater interactions
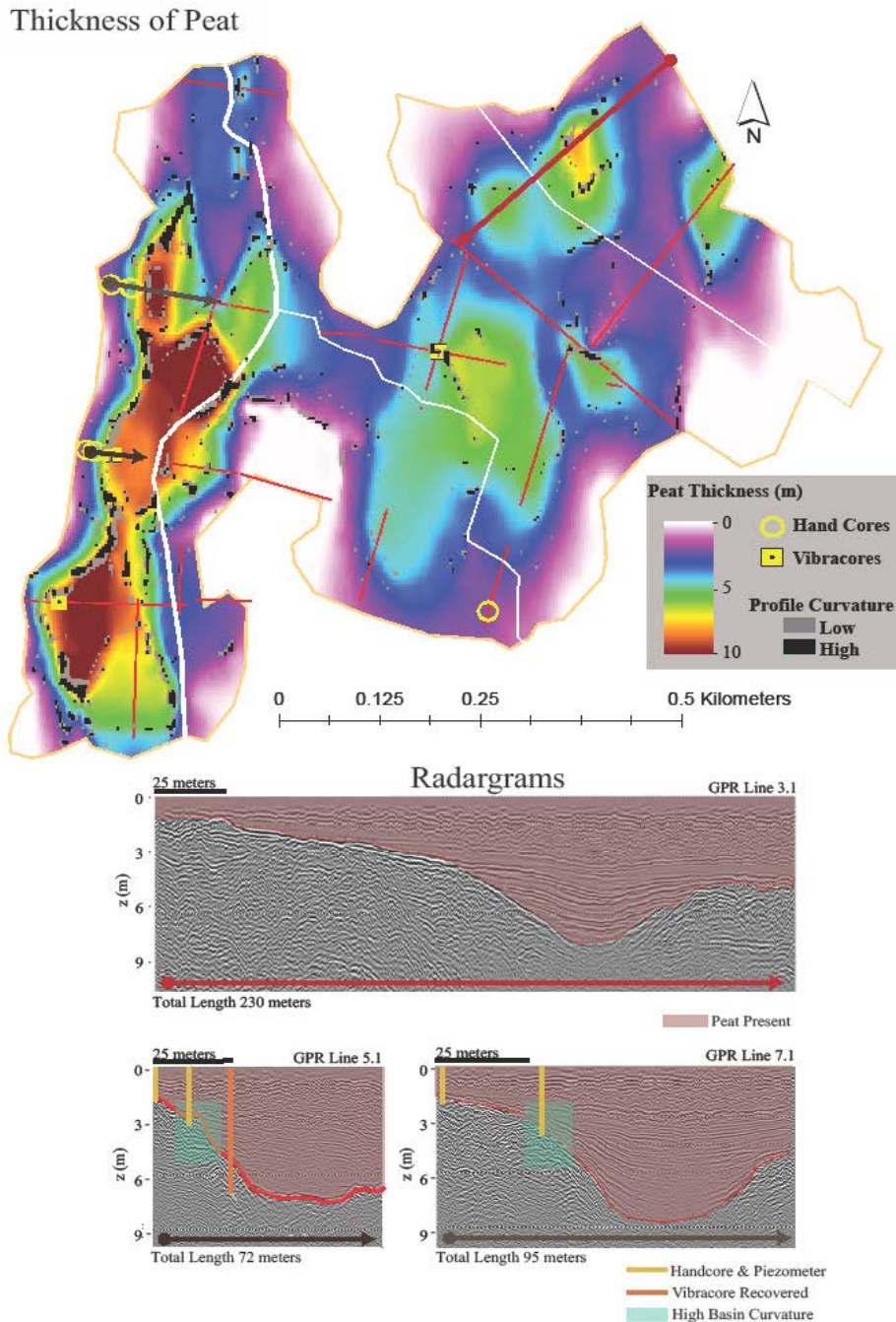
Figure 3: Site interpolation of GPR radargrams. GPR radargrams were used to create site-wide interpolation of the peat thickness as well as locations of high basin profile curvature. Western peat radargrams cross section show high basin curvature, indicated with the green boxes. The radargrams that are shown correlate to the same color arrows on the interpolation. Location of well and core installations are demonstrated within the cross sections.

(*Silliman et al.*, 1995; *Stonestrom and Constantz*, 2004; *Anderson*, 2005; *Constantz*, 2008; *Rau et al.*, 2014). Heat is a particularly good tracer to identify upwelling groundwater, as diurnal and annual temperature oscillations strongly influence surface waters, while groundwater temperatures remain relatively constant through time (*Constantz*, 1998). As heat propagates into the subsurface, the depth to which the surface water diurnal thermal signal penetrates is a function of the advective transport fluxes, heat capacity and conductivity of the saturated sediments (*Stonestrom and Constantz*, 2004; *Gordon et al.*, 2012). Thus, waters with high vertical seepage flux rates are less impacted by conductive diurnal signatures, as the upward advective force dampens the amplitude of the downward conductive diurnal signal (*Stallman*, 1965; *Goto et al.*, 2005; *Hatch et al.*, 2006; *Rau et al.*, 2014). Therefore, where significant upwelling is present, the surface thermal amplitude is dampened locally, which creates a thermal anomaly at the streambed where the magnitude of amplitude dampening is a function of the vertical flux rate and direction. If we know groundwater temperature and the surface temperature data we are able to determine relative flux estimates at varies seepage zones across the site.

Groundwater temperature is dependent on its temperature at recharge. While it is common practice to use the average annual air temperature plus 1 degree Celsius to determine average groundwater temperature (*McKenzie et al.*, 2007), this approximation may not be appropriate, particularly in strongly advective, low residence time aquifers such as the Plymouth-Carver (*Taniguchi*, 2002). In this case, it is more appropriate to determine a seasonal groundwater signal with a sinusoidal function to fit the annual cycle

and seasonal fluctuations. Temperatures were monitored at 15-minute intervals within a shallow well on the site (MW-1). From November 2012-March 2013 temperature ranged from 8.6 °C- 10.7 °C. We fit these data with a periodic function to predict the annual groundwater temperature signal for our study period (July-August 2013). We interpolated missing data along this function and determined that between July 1st - September 1st, 2013 the groundwater temperatures range from 9.5-10.5°C.

Surface water temperatures can be difficult to constrain, as they are dynamic, and can be modified by weather, channel morphology, near-stream vegetation, and local hydrology. *Swain et al.* (2012) also includes the soil heat storage as an important parameter in a wetland's heat budget. Water column buoyancy effects are also an important consideration when using thermal tracing techniques. Changes in water density due to temperature induce stratification in low gradient systems. This effect significantly affects to thermal mapping, and the effectiveness of different methods. Each temperature method we use requires unique analysis of the impact of these sources or sinks of heat on the data observed during different seasons, and is addressed within each method section.

At other wetland sites, seepage flux magnitudes and directions have been shown to be temporally transient (*Fraser et al.*, 2001; *Sebestyen and Schneider*, 2001). However, due to the consistent high hydraulic gradient in the regional aquifer (*Masterson*, 2009), we assume that temporal dynamics changes to flux are insignificant within our data set.

3.2.1. Fiber-Optic Distributed Temperature Sensing

Raman spectra fiber-optic distributed temperature sensing (FO-DTS) is becoming increasing popular for heat tracing use in aquatic systems, as this technology allows for high spatial temperature resolution (e.g. 1 m) along extensive linear cables (e.g. kilometers). FO- DTS provides continuous longitudinal temperature measures and has the ability to detect spatial variability in groundwater discharge, which point-measurements may miss (*Lowry et al.*, 2007; *Briggs et al.*, 2012). Data can be collected at a high temporal resolution over many days to weeks, and simple statistics such as mean or standard deviation can be applied to every meter along the cable to identify groundwater seepage and indicate its relative magnitude and permanence (*Selker et al.*, 2006; *Tyler et al.*, 2009; *Briggs et al.*, 2012). The FO-DTS system functions by initiating a laser pulse along optical fibers and then measuring the frequency and timing of backscattered light. Temperature is determined through an analysis of the Raman backscatter; the ratio of temperature dependent wavelength (Anti-Stokes) to the temperature-independent wavelength (Stokes) provides a measure of temperature continually along the deployed fiber optic cable in space (determined by the time of return signal) (*Selker et al.*, 2006). The longer data are collected in time the higher the precision (stacking), which increases proportionally with the square root of collection time (*Tyler et al.*, 2009). Tyler et al. (2009) provides a thorough review of the details of the technology.

In July and August of 2013 four FO-DTS deployments were performed, one within the drainage ditches of eastern peatland cells, and three within the western cells. We capitalize on the modified structure of the agricultural peatland surface, particularly

the relatively evenly spaced drainage ditches, to thermally sample surface water in a distributed way which is not possible in more natural systems (e.g. *Lowry et al.*, 2007). At the research site, drainage ditches are located every ~35 meters (Figure 2), providing an opportunity to map temperature over a more representative portion of the site and better constrain the locations and mechanisms of broad-scale groundwater discharge. Drainage ditches do induce an area of artificially lower hydraulic head within the peat (*Price et al.*, 2003; *Hoes et al.*, 2009); however due to the regular, close spacing of drainage ditches and low hydraulic conductivity at the site, any observed discharge are assumed to be representative of the surrounding +/- 17.5 meters laterally.

We chose deployment sites based on previous infrared surveys (November 27st, 2012), interviews with farmer, and feasibility of installation; and each deployment ranged from 1000m-2500m in length. Macrophyte growth was cleared during installation and continuously monitored through each deployment; large macrophyte shade, and also caused the fiber-optic cable to be suspended near the surface at a few locations. Temperature data were collected and averaged over 15 minute intervals with Sensor Tran Gemini HT control unit in single-ended mode. This FO-DTS unit allows for 1-meter spatial accuracy at 0.1°C precision at ~ 15 min integration timescales, and the integration time of 15 minute provides ample data points to determine a diurnal temperature signal. Each FO-DTS deployment was run for a minimum of 5 days to ensure multiple strong diurnal signals were captured. Fifty-meter calibration coils were maintained at a constant temperature with an ice and/or ambient bath and were compared to an independent Onset HOBO Water Temperature Pro v2 Data Logger (U22-001) (± 0.2 °C accuracy).At every

time step the temperature offset between the calibration baths and recorded temperature were subtracted. Trending caused by decrease of light recovered as a function of length was removed with the Sensor Tran Software.

Two main methods were used to identify groundwater seepage with FO-DTS: average temperature and standard deviation over time. The mean temperature was determined for each meter along the cable for each survey to identify spatial low temperature anomalies indicative of groundwater temperature during July-August 2013. This is an appropriate because the average surface water temperature during this period was distinct from the groundwater's thermal signature. Another method to identify groundwater discharge was using standard deviation of temperature as groundwater temperature remains constant through time (for the period of the deployment) and surface water temperatures fluctuate daily, therefore groundwater discharge zones may be characterized by relatively low variance compared to "ambient" surface water. To achieve this analysis the temporal component of the FO-DTS data was analyzed for each meter, and we used the standard deviation over the deployment period to determine the influence of the diurnal air temperature signal on each location. Locations of low standard deviation (σ <1.5) were predicted to be a groundwater seep. This method is desirable as it is a simple statistic that can be applied efficiently across all deployments, and provides an indicator independent of absolute temperature. We use both the average temperature and the standard deviation of the temperature, as these metrics together provide a more comprehensive understanding of the seepage dynamics across the site.

3.2.2. Infrared Surveys

An infrared camera is a remote sensing, high-resolution device that is able to record and quantify surface infrared (heat) radiation. Thus, this technology is very applicable to environmental groundwater surveys because of the scale of interest and potential thermal contrast between groundwater and surface water (*Loheide and Gorelick*, 2006; *Chen et al.*, 2009; *Deitchman and Loheide*, 2009; *Briggs et al.*, 2013), particularly at large sites, or sites where in-situ measurements are not possible. The hand-held infrared camera survey was conducted to both expand the thermal survey and to compare this method to the FO-DTS data. We used a high-resolution forward-looking infrared camera (T640BX model FLIR, FLIR Systems, Inc.) with GPS and compass capabilities borrowed from the U.S. Geological Survey. The infrared (IR) survey was useful as it allowed for efficient spatial coverage, and allowed us to obtain thermal data unreachable with FO-DTS due to long distance or dense growth. As mentioned above, FO-DTS installation can be labor intensive, invasive, and not feasible in highly vegetated environments, while the IR surveys are quick, and only spatially limited to where the operator can access. However, infrared surveys only image the surface ('skin') temperatures, and in low gradient systems if there is stratification due to thermally induced density differences, the IR image may not be able to capture cooler seepage inputs. This is only of major concern when the groundwater is cold in relation to the surface temperature (summer) as the buoyancy forces of the cooler water cannot overcome the overlying pressure head to be observed at the surface. Therefore, as FO-DTS cables are installed on the streambed, FO-DTS may be a better indicator of seepage during the summer months. Winter surveys are more effective for IR surveys as the

warmer groundwater rises to the surface allowing clear IR imagery. In low gradient systems there is less mixing, and the shallow drainage ditches makes this site an ideal for exacting locations of groundwater input with IR.

At Tidmarsh farms three IR surveys were completed, one survey during July 30th and 31st , 2013; a smaller survey completed March 21, 2014; and one reconnaissance survey on November 27th, 2012 that was not included in the quantitative evaluation due to a GPS lag, but was used to locate potential FO-DTS deployment locations. The July surveys were used to make comparisons to the FO-DTS data as it was taken at the same time period; the March survey was used to compare the impact of buoyancy on IR images, and describe any seasonal variability in seepage patterns. We observed strong buoyancy effects at the site, so all summer survey image locations were manually mixed before an image was taken; however a distinction between surveys should be made. The time the summer surveys were completed was after 2100 and the winter survey was done between the hours of 0600 and 0800 as to minimize the influence to surface reflection. At the time of the summer surveys groundwater was approximately $10.1^{o}C$ and the air temperature was $20\ ^{o}C$; therefore, in the IR images the groundwater seepage is shown as cold anomalies (Figure 4). In the March surveys, groundwater was $8.7^{o}\ C$, and the air temperature was $3\ ^{o}C$, therefore groundwater seepage is shown as warm anomalies in the thermal images (Figure 4).

Each IR image provides a wealth of information, and, while these are useful
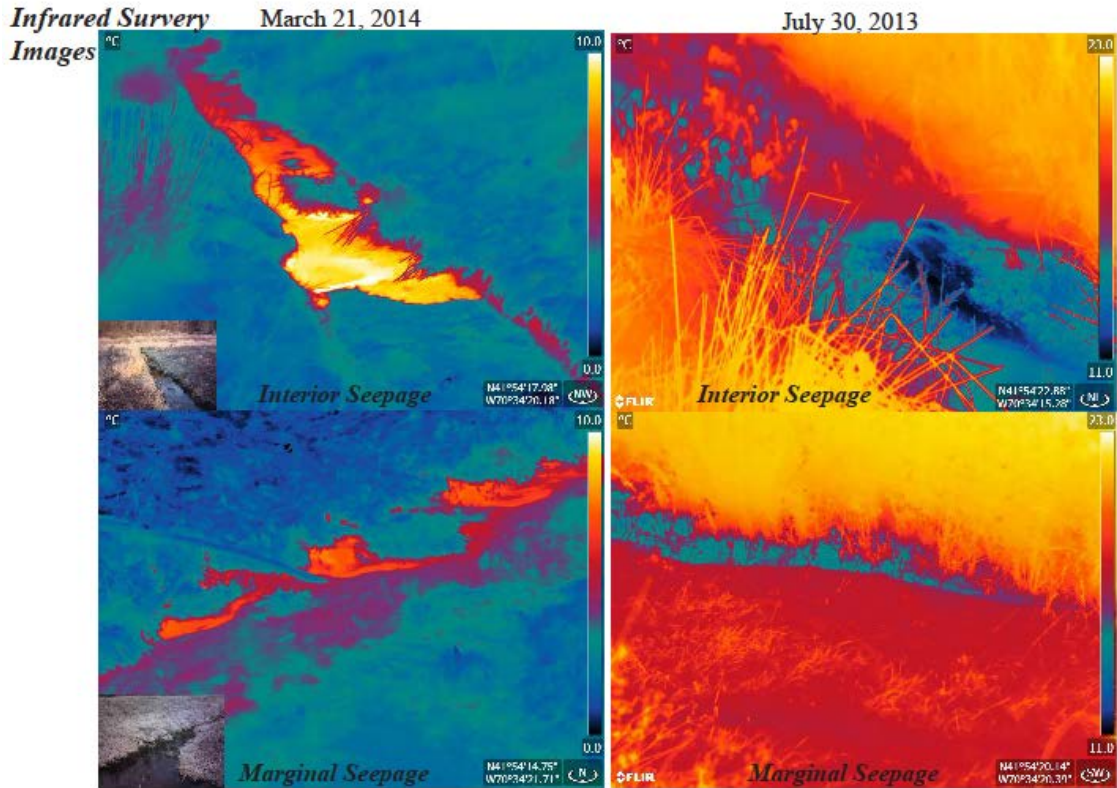
Figure 4: Forward-looking Infrared images from two distinct seasons: summer (July) and winter (March). In March, the groundwater is a warm anomaly, and in July, the groundwater is observed as a cool anomaly. Each figure shows an example of interior seepage or marginal seepage.

individually, it is cumbersome to evaluate all the images together. Therefore, to create a spatial figure that incorporates the useful data from each of the IR images for the entire site, we simplified each image to a single point represented by a single color. The single color symbolizes a point temperature measurement that is manually chosen from each IR image based on the user's personal knowledge. This single representative temperature pixel is chosen to select the water surface, and to avoid distorted images and land influences. If a thermal anomaly (closer to groundwater temperature than the surrounding waters) was present within the image, a temperature pixel was selected from

that location, otherwise a surface water pixel was chosen that represented the water temperature for the image. We developed a direct program to then transcribe each of these chosen pixels into Google Earth© using the location of the camera when the image was taken and the selected pixel color; thereby producing a site map of the temperature at the location of each survey image and the directionality of the shot. This allowed unprecedented automated generation of georeferenced IR data which could be used quantitatively to evaluate spatial seepage patterns and the relative magnitude of seepage rate based the similarity of the seepage temperature and the groundwater temperature.

3.2.3. Temperature Profiles

The depth to which the surface diurnal signal can penetrate saturated near-surface sediments is a function of the period of the signal, the fluid flow velocity and direction, and fluid-saturated sediment physical properties (*Stallman*, 1965; *Goto et al.*, 2005; *Hatch et al.*, 2006). With depth, the diurnal surface heat sinusoid decreases in amplitude and phase shifts forward in time. Modifications from a purely conductive signal are attributed to advective fluxes, and using a one dimensional heat transport equation simple analytical solutions can be derived with specified boundary conditions to solve for fluid flux (*Stallman*, 1965; *Silliman et al.*, 1995; *Hatch et al.*, 2006; *Schmidt et al.*, 2007; *Rau et al.*, 2014).

We installed four temperature profilers at our site to understand the vertical subsurface fluid flux patterns. Maxim ibuttons sensors (0.0625 °C resolution; 1°C accuracy) were placed along a wooden dowel, four beneath the peat surface at -2.5, -5.0, -

33

10.0, -25.0 cm depth and one at +2.5 cm above the surface. We coated each ibutton with silicon sealant to prevent leaking/sensor damage; however still experienced a high degree of sensor failure. A 10-minute sampling rate was used for a minimum of 7 days during July and August of 2013 to create each temperature time series.

Installations locations were chosen to represent the two types of seepage that were first observed with the FO-DTS, and the two control deployments were installed within drainage ditches. All deployments overlapped with FO-DTS data and/or IR imagery. In the absence of strong diurnal signal propagation, such as that expected below stratified drainage ditches, steady-state heat-flux analytical solutions based on measured surface water interface, groundwater, and intermediate-depth temperatures can be used to estimate seepage flux if the system is assumed to be at quasi steady-state (*Schmidt et al.*, 2007). So, due to its simplicity and minimal boundary condition requirements, we chose to use the analytical solution to the heat transport equation derived by *Turcotte and Schubert* (1982) and modified by *Schmidt et al.* (2007) to approximate upward seepage:

$$q_z = \frac{K_{fs}}{\rho_f c_f z} \ln \frac{T(z) - T_L}{T_0 - T_L} \tag{1}$$

The thermal conductivity (K_{fs}, J s^{-1} m^{-1} K^{-1}), is calculated using the geometric mean of the thermal conductivity of the solid, and the fluid:

$$K_{fs} = K_s^{(1-n)} \times K_f^n \tag{2}$$

Where K_s is the thermal conductivity of the solid, which is peat at our site, K_f is the thermal conductivity of the fluid, and n is the porosity of the matrix. The density of the fluid and heat capacity of the fluid multiplied together are the volumetric heat capacity of the fluid ($\rho_f c_f$, J m^{-3} K^{-1}).

K_S [J s^{-1} m^{-1} K^{-1}]	0.4[a]
K_f [J s^{-1} m^{-1} K^{-1}]	0.6[b]
n	0.5[a]
ρ_f at 10°C [kg m^{-3}]	999.7
c_f at 10°C [kJ kg^{-1} K^{-1}]	4193

[a] *McKenzie et al.*, 2007; [b] *Schmidt et al.*, 2007

Table 1: Parameter values used for to calculate the steady-state heat-flux analytical solution

After these parameters are established, we are left with three unknowns: groundwater temperature (T_L), a fixed temperature at z=0 (T_0), and a temperature at depth z (T(*z*)) to determine a vertical flux estimate.

We recognize that the temperature value we use for T_0 is from the in-stream thermistor that was located at 2.5 cm, not flush with streambed (0cm); therefore, any stream column thermal stratification will distort our calculations of thermal gradient ($\delta T/\delta z$) and influence the flux estimate; therefore, these flux values are used with caution.

3.3 Groundwater Flow Path Source Identification

Groundwater source information can give insight into the direction of groundwater flow, linked aquatic systems, and potential contaminants. These potential impacts are important for local and regional water resource managers, as modifications to one part of the system may affect the ecosystems along the flow path, and may induce unintended consequences. To trace the source of the waters, we use stable water isotopes, both $\delta_{18}O$ and δ_2H, as these isotopes help us distinguish between local recharge and regional recharge. This helps us understand the flow paths surrounding the site, and the directionality of the hydraulic gradients that are inducing the anomalous pressures causing seepage. As our hypothesis predicts that seepage distribution is caused by the perpendicular intersection of groundwater flow and steep basin structure, the source waters are important to identify.

3.3.1 Stable Water Isotopes

Water stable isotopes as a tracer use the water molecule itself as an indicator of the recharge environment. The water molecule is composed of two elements that both have at least one isotope (Oxygen: ^{18}O (0.204%), ^{17}O (0.037 %), ^{16}O (99.7 %); Hydrogen: ^{2}H (0.015 %), ^{1}H (99.9%)). The isotopic composition of water is stated as the ratio of the heavier isotope to the lighter isotope (e.g. $^{18}O/^{16}O$) per mil relative to the Vienna-Standard Mean Ocean Water (VSMOW).   The relative abundance of each isotope within a water molecule changes due to thermodynamic reactions caused by mass fractionation. Stable water isotope fractionation is dependent on air temperature, altitude, latitude, distance inland, and humidity (*Kendall and Coplen*, 2001). If multiple flow path sources vary substantially stable water isotopes can be used to "finger-print" the contributing

source to the location in question (*Hunt et al.*, 1998; *Drexler et al.*, 1999; *Blasch and Bryson*, 2007). At Tidmarsh Farms we analyze groundwater seepage for unique fractionation signatures/patterns, indicative of regional precipitation or ^{18}O enriched evaporative signatures (trends that fall right of the meteoric line). The enriched signatures are thought to be recharged from nearby lakes, rather than the meteoric waters from the regional uplands. As most lakes are to the south of the site, an enriched groundwater signature would imply a northern flow path, rather than the regional east/northeast flow path. By identifying the groundwater flow path source of a sample, we are able to approximate the direction of hydraulic gradient responsible for supplying the sample location.

3.3.2 Isotope Sample Collection and Analysis

Isotopic analyses were performed on water samples collected from surface water (monthly), shallow ground water (seasonally), deep groundwater (seasonally), groundwater seepage (August 2013) and pore waters (October 2013). Each sample, excluding pore water samples, was filtered and bottled in the field. Upper 1-meter peat pore water samples were acquired through a manual press of samples from Russian peat cores, and subsequently filtered for analysis. To analyze each water sample, we used an in-house high precision Picarro L2130-*i* Analyzer, and used the recommended six analyzes per sample, discarding the first three values as to prevent memory over-printing. Three separate standards were used, all which maintained relative uncertainties of less than 0.001% and 0.02% for δ_{18}O and δ_2H respectively through all the isotopic analyses.

The USGS has historically monitored groundwater isotopic compositions at numerous well locations and depths within the PCKD aquifer, which gives approximation of the regional groundwater values for the aquifer and the expected annual range of local precipitation (local meteoric water line) (supplemental materials). The meteoric line at the site was created by creating a linear regression through the regional aquifer USGS isotope data. The local meteoric line differs from the global meteoric line ($\delta_2 H$ = $8.17\delta_{18}O$ +11.27) because of distinct vapor sources, elevation, rainfall seasonality, and humidity differences. As the deep groundwater site samples exhibit an evaporated signature we can identify the regional and local flow path as two end-members, and then trace the source the flow paths that feed each sample to a specific end member.

4.1 Resolving Peatland basin Structure

4.1.1 GPR Survey

The interpolation generated from the GPR transects depicts four isolated depressions at the site; two depressions in the east cells and two in the west cells. The combined surface area of the east cells is ~ 0.32 km^2, and they have a maximum peat thickness of ~6 meters with gradual basal peat slope changes- low curvature values (Figure 3). In contrast, the west cells show a maximum peat thickness of ~10 meters, and a surface area of ~0.12 km^2. The basin structure of the west cells is more complex than eastern cells, as the west cells have observable undulations in the basal peat/sand contact, with steep slopes, and high curvature resulting from dramatic changes in basin shape. Figure 3 shows the distribution of high basin curvature zones interpreted from the GPR surface; there is a notable high curvature zone along the western edge approximately 30 meters from the edge. The GPR profiles exhibit multiple series of normal faulting beneath the peat body indicative of ice melt-out/collapse features (Figure 3); supporting the theory of kettle pond origin. These faults are expected as the ice block melts the outwash sediments that have accumulated above collapse into the melt-out depression creating faulted blocks surrounded by steeply dipping normal faults (*Kruger et al.*, 2009).

All recovered cores have a clear acrotelm/catotelm boundary, as well strong degree of heterogeneity in decomposition degree with depth; there are also intermittent

strong vegetation changes, such as layers of woody debris. The degree of decomposition generally increased with depth, noted by a decreasing ability to recognize plant species or intact specimens; therefore, a strong decrease in hydraulic conductivity with depth was qualitatively assumed. The base of the western cores had an undetermined fine, grey/brown substance, and could not be distinguished as either organic or mineral-based, but did exhibit clay-like tendencies. There were few identified sand layers without any observable grading (below the surficial anthropogenic deposits), indicating storm deposits or bank collapse. In two of the three vibracore cores we were able to recover the glacial sediments beneath the peat, and describe them as well-sorted, medium-coarse sand deposits, typical of outwash facies.

4.2 Relating subsurface basin structure and groundwater seepage distribution

4.2.1 Fiber-optic distributed temperature sensing

The FO-DTS dataset provides us with a detailed overview of the temporal and spatial distribution of the summer temperatures in peatland surface-water. Measurement cables were installed along the edge and center drainage ditches as well as the main channel to achieve thermal sampling of the typical environments across the site. Deployments were concentrated within the western cells, as more seepage was previously observed there with infrared imagery collected during November 2012. In addition, the more complex nature of the western basin, as well as the western basin's perpendicular intersection with the regional groundwater provided a good location to test our hypothesis thoroughly.

.

Relatively low thermal variance can be a strong indicator of groundwater seepage as groundwater is thermally stable in comparison to surface water (*Lowry et al.*, 2007); therefore, upward seepage zones typically decrease the standard deviation of temperatures collected along the bed. Average temperature can also be a useful indicator of groundwater input during seasons where the air temperature and groundwater temperature are disparate (winter and summer), as waters with groundwater inputs will appear as strong thermal anomalies. A relative estimate of flux rates can also be made, as higher groundwater fluxes will typically more closely resemble the groundwater temperature. We use both of these simple statistics (standard deviation and average temperature) to characterize each FO-DTS 1m sample location and to locate seepage.

We analyze the two non-seepage aquatic environments observed at the peatland surface: the well-mixed main channel, and the "ambient" drainage ditches that showed thermal patterns strongly forced by diurnal air temperature swings. For the Cell 3 FO-DTS deployment (July 27-29th, 2013) the mixed main channel's average temperature is 16.9 °C, and the drainage ditches in non-seepage zones typically exhibit an average temperature of 23.8 °C. These relationships were typical over the four FO-DTS deployments. Groundwater was determined to be 10.1 °C during the deployments using sinusoidal interpolation from earlier season data. Figure 5 shows the selected example time series of the main channel and ambient drainage ditch. Both these environments have a strong diurnal signature and exhibit high standard deviation.

Distinct from the main channel and ambient drainage ditch environments we identified two categories of thermal anomalies: 1) zones that show low standard deviation and an average temperature in between ambient surface-water and groundwater; 2) zones that show low standard deviation *and* an average temperature close to groundwater. These two kinds of statistical anomalies were unique because they did not appear as a spatial continuum rather at distinct locations, and are identified as groundwater seepage. The first type of seepage only appears along the periphery of the peatland and therefore we refer to these locations as 'marginal seepage'; the second type of seepage zone occurs predominately within the peat platform and we refer to these as 'interior seepage'. Specifically, marginal seepage has a relatively low standard deviation through time, and an anomalous heat signature approximately 3-5° C warmer than groundwater temperature during the summer; the interior seepage also has a low standard deviation, but more closely matches groundwater temperatures (10.1^{o}C) (Figure 5). These are similar to the "point" and "diffuse" peat seepage categories defined by Rossi et al. (2012), and indicate relative seepage rates are higher at interior locations because water temperatures more closely resemble the groundwater source.

Figure 5 shows the time series of four separate FO-DTS sampling meters over three days: marginal seepage, interior seepage, typical ambient drainage ditches, and the main channel all within Cell 3. There are strong distinctions between these four environments, including the consistent difference between marginal and discrete seepage temperatures. As discussed above, seepage zones exhibit low standard deviation in
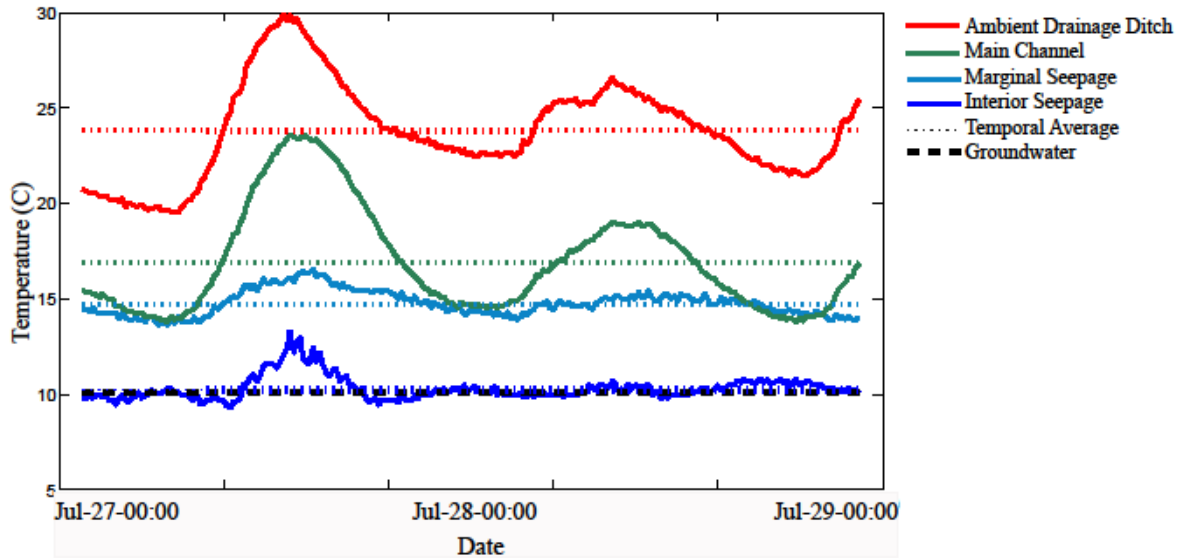
Figure 5: FO-DTS time series data sets for four separate meters within Cell 3. Each of these sample locations provide an example of the four common thermal observations: ambient drainage ditches with high average temperatures and large amplitude; mixed main channel data has a lower thermal average and large amplitude; marginal seepage has a similar average to the main channel, but has a low amplitude; and interior drainage has a groundwater temperature average temperature and low amplitude.

comparison to the main channel and the drainage ditches. Also, the average temperature of both seepage is lower, and closer to the groundwater temperature, with interior seepage zones being coldest. Although all the FO-DTS were deployed along the streambed, the water depths were not consistent, which could explain some temporal phase shifts observed within the data, and slight changes to the standard deviation between similar locations. However, as seen in Figure 5, the four types of time series could still be distinguished using both average temperature and standard deviation. Due to the low topographic gradient, persistent low standard deviation, and the isolated occurrence of these two thermal anomalies, we are confident that these two types of thermal anomalies spatial segregated between the margin and interior are not due to groundwater and surface mixing rather are two distinct processes. Figure 6 shows the

average temperature over the deployment, and the standard deviation of temperature for each meter along the cable. Standard deviation is indicated with the relative size of the plotted symbol; the larger the standard deviation the smaller the symbol; therefore temporally stable groundwater seepage locations are shown with large symbols to accentuate possible seepage zones. Marginal seepage (σ<1.5 and 13-15°C) are shown to dominate the edge of the peat and appear within the first ~ 30m interior of the peat margin. Interior seepage appears sporadically along the peat edge, but most notably within the interior of the peat surface ~30 m from the peat margin. At these interior locations, there is no observable seepage, neither marginal nor interior seepage, more center of this seepage point (Figure 6). When these data are overlain on the high basin peat curvature map, generated through the GPR survey, abrupt seepage end and/or interior seepage presence coincides with locations where the peat rapidly thickens. This is observed on both sides of the western subsurface basin; however, it is more widespread on the western edge of the western cells, particularly in the southwest portion of the site (Figure 6). Seepage in this area is so prolific it is difficult to differentiate between marginal seepage expressions and interior seepage mixing with surface waters, but the relation to high basin curvature is apparent. This correlation provides insight into the sub-surface structural forcing of seepage patterns across the site.

Ambient drainage ditches show high standard deviation and warm average deployment temperatures (Figure 5). These locations indicate surface water with no significant groundwater seepage influx. There are drainage ditch locations that exhibit a low standard deviation close to that of marginal and interior seepage, but warm average

temperatures. This could be a result of thermal stratification, very low flux zones, or marginal seepage through longer, oblique flow paths through the upper 100 cm of the peat. However, it does not fit our objective of identifying thermally stable inputs for ecosystem stability and are not discussed further. Additionally some FO-DTS sample locations had an average temperature near groundwater temperature, but have a high standard deviation. This could likely be due to a number of factors: shallow drainage ditch causing the albedo of the black cable to record diurnal signatures; localized seepage small in comparison to the 1m resolution sampling method; or the cable did not remain underwater for the entirety of the record. Even though these locations show strong correlation to the high basal peat curvature they were not included in the final seepage analyses to achieve consistency in our seepage identification method.

4.2.2 Infrared Thermal Surveys

The remotely-sensed (hand-held) IR surveys covered a large area more quickly than the FO-DTS deployments; this allowed for better spatial coverage of the peat surface, and allowed for multiple thermal surveys over different seasons. IR images report a high-resolution record of the infrared radiation at each sample location, and we transcribed the images' thermal signature at points of interest onto a site map allowing better large-scale visualization and interpretation of this data and making IR results spatially comparable to FO-DTS results. The surface expression of marginal seepage are warmer than groundwater in the summer and cooler than the groundwater in the winter, making a clear distinction between marginal and interior seepage, as interior seepage maintains groundwater temperature throughout the year. The winter infrared survey
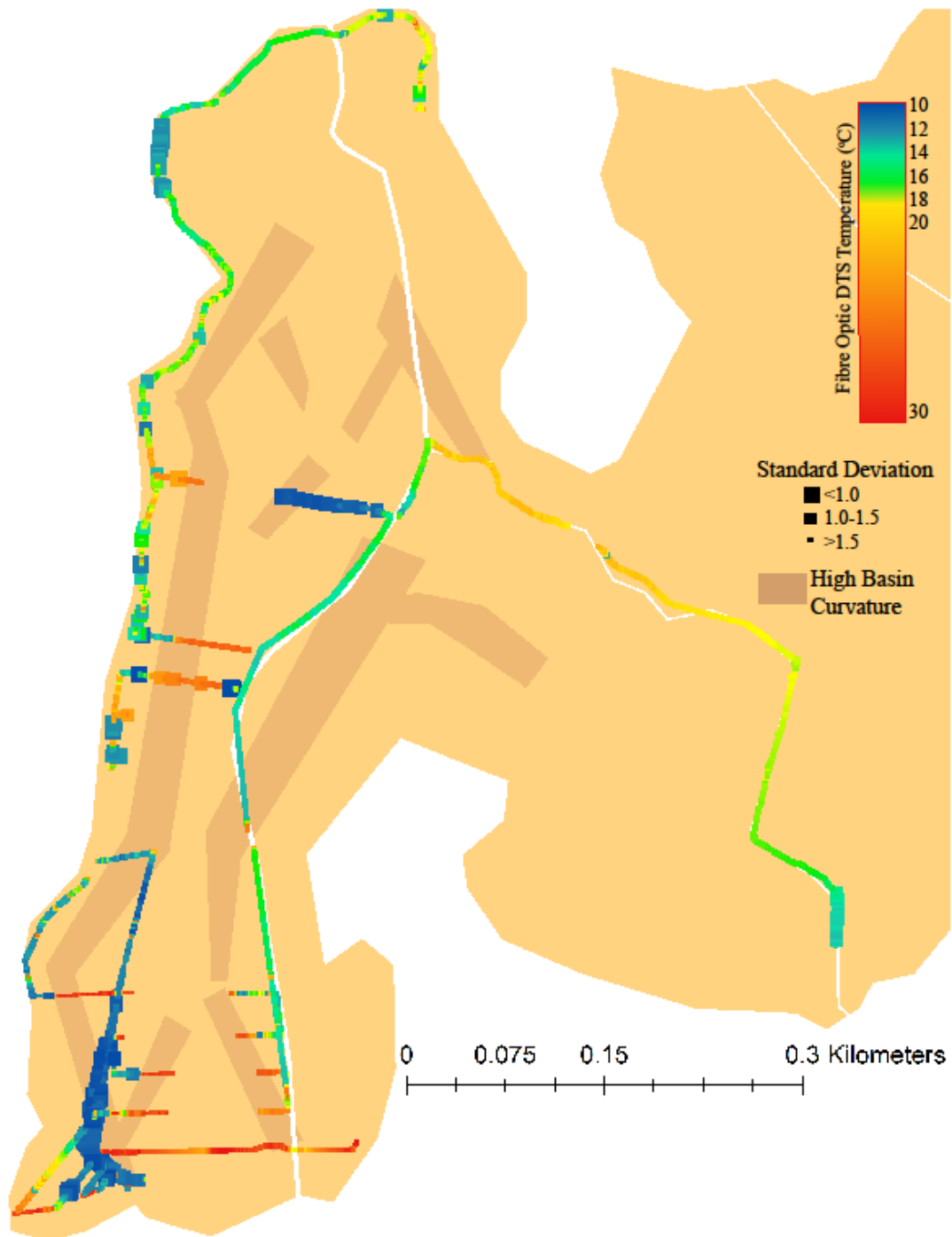
Figure 6 : Map view of average temperature and standard deviation for all four FO-DTS surveys at the Tidmarsh site. Locations with low standard deviation and groundwater temperatures are identified as locations of groundwater seepage. High basin curvature generalizations that are shown are the locations of high basin curvature shown in figure 3.

provided a successful determination of both types of seepage as the air temperature was consistently distinct from both seepage temperatures, and, due to lower density, the warm seepage showed a surface expression that was easy to isolate from surrounding surface water in each image. In general, spatial plots of IR data showed similar results to the FO-DTS spatial plots and both marginal and interior seepage types were observed (Figure 6 & 7). Comparable IR thermal anomalies of both marginal and interior seepage types were captured in the winter and the summer (Figure 4), yielding confidence in these seepage distinctions.

Similar to the FO-DTS observations, marginal seepage ceases at a distance from shore coincident with high basin curvature, and interior seepage is more common along high curvature zones. The infrared images show that marginal seeps occur in clusters along the margin of the peatland (Figure 4). Figure 7 shows that these marginal seeps extend into the peat cell until a threshold is reached at where no seepage is observed interior-of that point, typically 20-30 m from the edge of the peatland. There is no observable change on the land that correlates to this dramatic change. It is also observed that interior seepage typically occurs at this same threshold location. This spatial seepage threshold point correlates with the high basal peat curvature, replicating the observations recorded with the FO-DTS survey (Figure 6). The repeatability of these two distinct seepage types locations, between multiple methods and seasonally, indicate that unique hydrodynamics control each of these seepage types, creating distinct surface expressions.

During the March infrared survey a wet location on the interior of the northwestern cell was discovered that contained a plethora of ~1-5 cm diameter

47
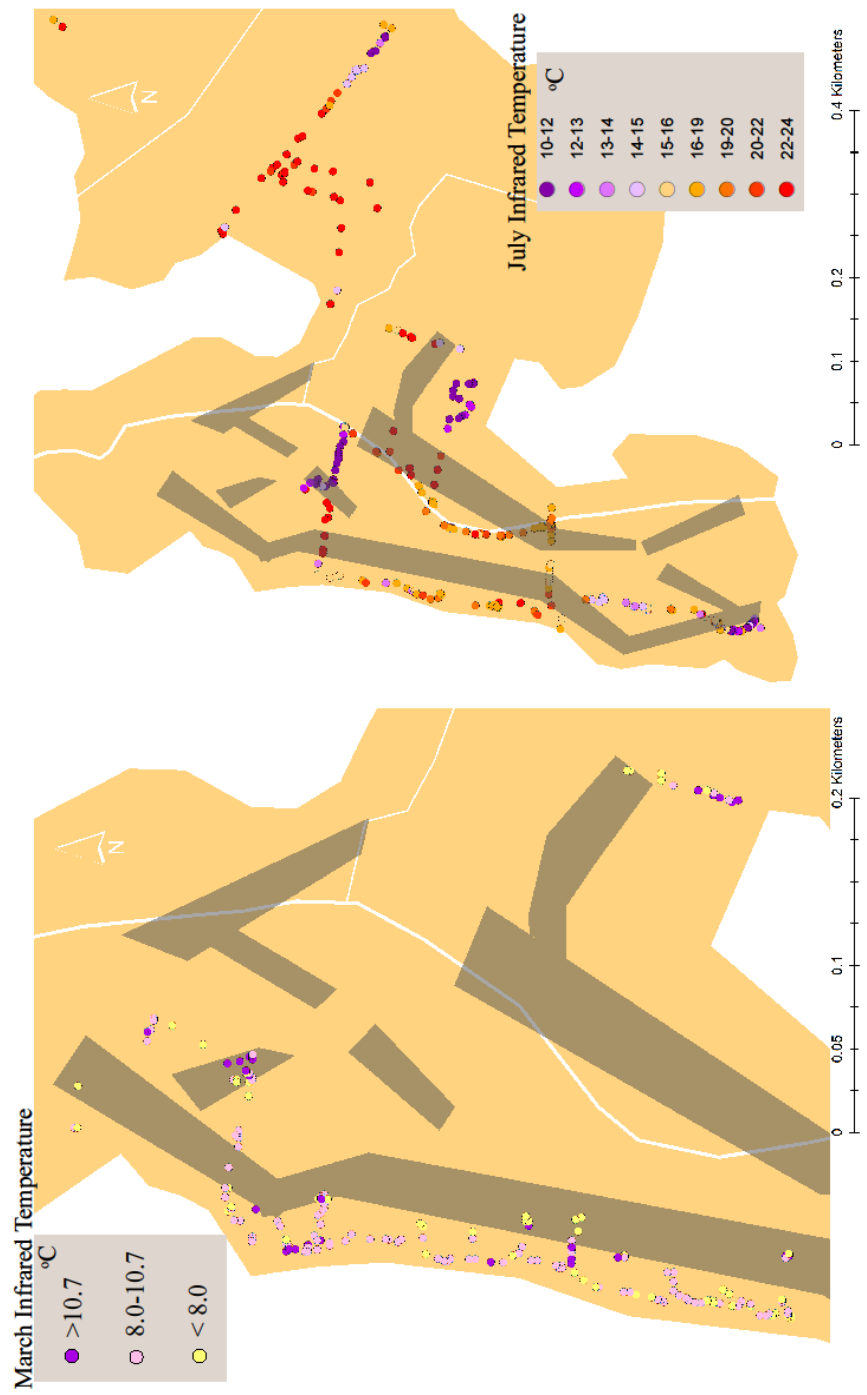
Figure 7: Tidmarsh Farms' March and July infrared surveys with thermal anomalies within the respective seasons. Each symbol indicates the location the image was taken from, and the color represents the surface water temperature determined through manual inspection of the images. Seepage zones are indicated by temperatures close to groundwater temperatures (~10.7 °C annually).

48

macropores within the peat and groundwater was discharging from the pores with typical "interior" seepage temperatures (Figure 8). This observation is similar to the peat macropores or 'peat pipes' described in previous peatland research (e.g. *Holden*, 2004; *Smart et al.*, 2012; *Cunliffe et al.*, 2013; *Vandenbohede et al.*, 2014), but the amount of macropores in this one location makes the northwest cell macropores observation unique for this site. This kind of density of visually discrete groundwater discharge locations were not observed elsewhere at the site, but linear FO-DTS data would not have been able to record lateral spatial distribution of these discrete inputs. The peat thickness map (Figure 3) indicates that the zone of high macropore density is an area of peat thinning reaching a minimum peat thickness of 3 m, and a location of high curvature (center of cell 3). Rossi et al. (2012) describes similar correlation to peat thinning at their site in Finland.
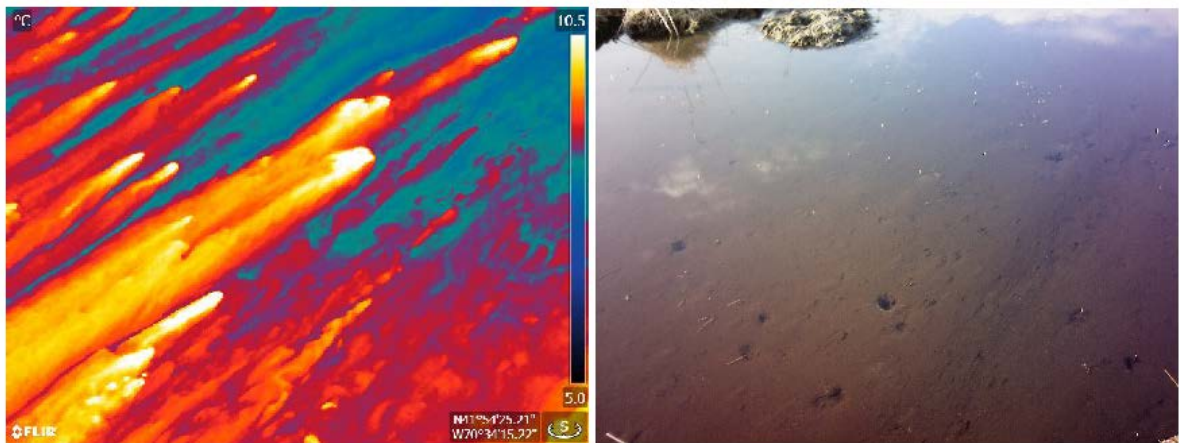
Figure 8: Infrared and camera image of a cluster of interior seepage. The peat basin shape beneath this image has a dramatic basin slope change, and the peat is 3 meters thick. This type of seepage is what has been described in previous research as peat pipes.

4.2.3 Subsurface Temperature Profiles

A marginal seep, an interior seep, and two ambient drainage ditch locations were monitored with 1D temperature profiles for 7-10 days. These profiles were installed with the goal of calculating flux estimates using analytical models of coupled water and heat flow. The temperature results from the four temperature profiles exhibited a different behavior from each other; however, all the temperature profiles, including the "ambient" drainage ditches, indicate upwelling of groundwater. This is determined as there is rapid attenuation of the diurnal signal with depth, and all the profiles have the characteristic convex shape of mean temperature with depth (Figure 9)(*Schmidt et al.*, 2007). As Conant (2004) demonstrates, a temperature profile under a no flow, conduction only scenario would show a linear mean temperature gradient change with depth from surface water to groundwater temperature. The greater the groundwater flux to the surface the more convex the mean temperature gradient becomes, compressing the diurnal envelope towards the surface. In areas of strong expected seepage, such as interior zones, groundwater-like temperatures are expected over the entire sub-surface profile as diurnal signal penetration (conduction from the surface) will be minimized.

We installed temperature profiler 1 in a location of marginal seepage determined with FO-DTS. This marginal seepage shows a surficial temperature of 13-14 ^{o}C in August 2013. The diurnal signal attenuates moderately, converging on seasonal groundwater temperatures at approximately - 25 cm in a convex pattern; the total peat thickness at this location is 50 cm (Figure 9). Consistent with groundwater upwelling
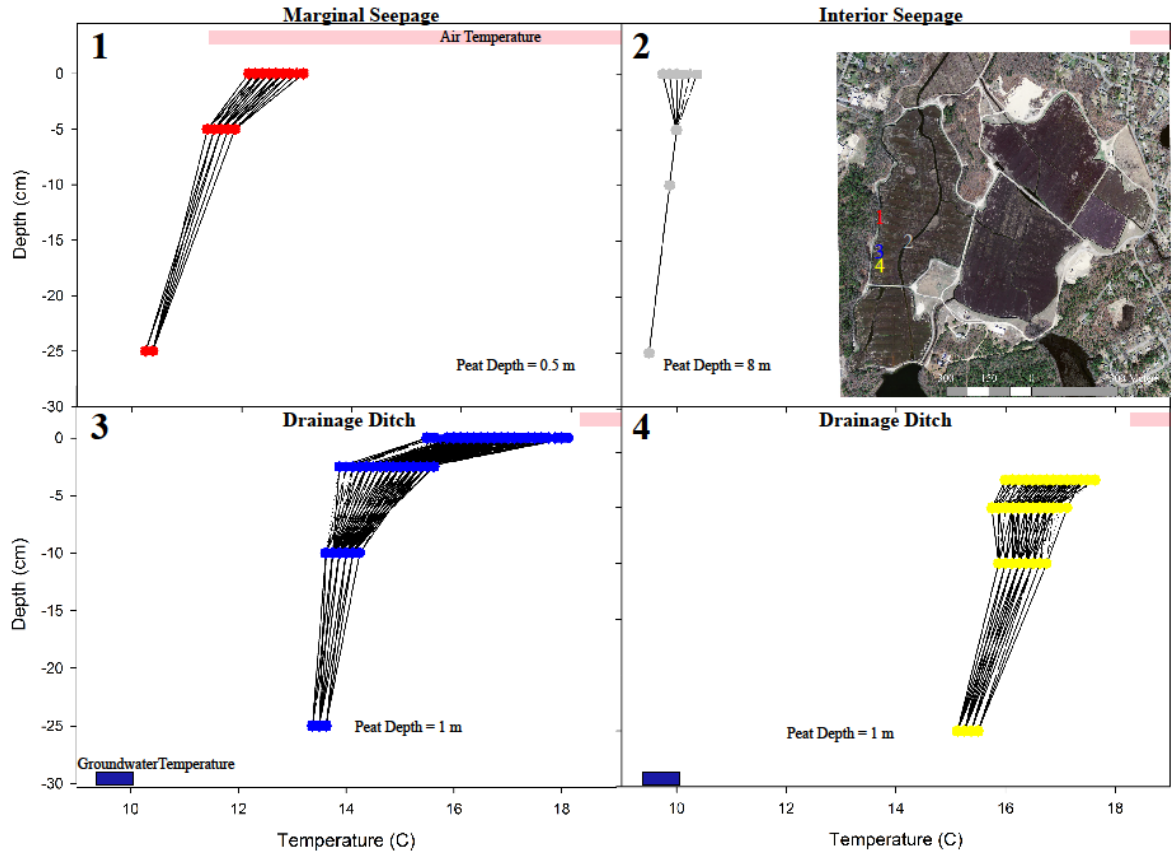
Figure 9: Thermistor depth profiles of the two identified seepage types: marginal and interior, and two ambient drainage ditch locations. The concave shape of the temperature with depth exhibited in 1-3 is indicative of upward seepage. The shape shown in 2 (interior seepage) indicates the strongest upward flow, followed by 1 (marginal seepage).

locations, there is little diurnal signal propagation at the seepage sites (Figure 10), perhaps due to thermal stratification in the slow-flowing ditch above, indicated by relatively low variance in the local surface water. Therefore, the analytical models which capitalize on the propagation of the diurnal signal with depth (e.g. *Hatch et al.*, 2006) could not be applied consistently, and consequently, we use an analytical solution that utilized a steady state upper boundary (Equation 1).

The solution results indicate that there is a modest 0.23 m d^{-1} flux through the peat at the marginal seepage location, which is consistent with diffuse, modest upwelling

according to *Conant Jr.* (2004). In comparison, Profiler 2, which was installed in a location of interior seepage, exhibits a groundwater thermal signal throughout the entire profile, even close to the interface; the streambed thermistor (2.5 cm) showing very slight thermal shifts (σ= 0.096°C), which are very near to the resolution of the instrument (0.0625°C). This unique temperature profile is indicative of very high upward flux rates, as the diurnal signal cannot be resolved and there is essentially no downward conduction from above. Because there is essentially no thermal gradient at this interior seepage site we were unable to use the *Turcotte and Schubert* (1982) solution, however this condition indicates very high upwelling flux in comparison to the marginal seepage to maintain this thermal depth profile (*Conant Jr.*, 2004).

The two other temperature profilers (3 & 4) were installed as control thermal profiles in drainage ditches between the interior seepage and the marginal seepage deployments where the peat is 1 meter thick (determined by GPR data). Temperature profiler 3 results exhibit similar upwelling patterns within the temperature profile to the marginal ditch (e.g. convex profile) (Figure 9); however, temperatures more closely resemble surficial temperature than that of marginal seepage temperatures. This indicates upwelling groundwater discharge, but with a longer or more horizontal flow path at profiler 3 than the marginal seepage (profiler 2), which was more affected by surface thermal conduction. The presence of seepage demonstrates a major limitation of the FO-DTS and infrared reconnaissance surface temperature methods: upwelling is difficult to identify when the discharging water is similar to surface water temperature. The steady-

state solution provided by provides a flux rate of 0.20 m d^{-1}, nearly identical to that of the much cooler marginal seepage.
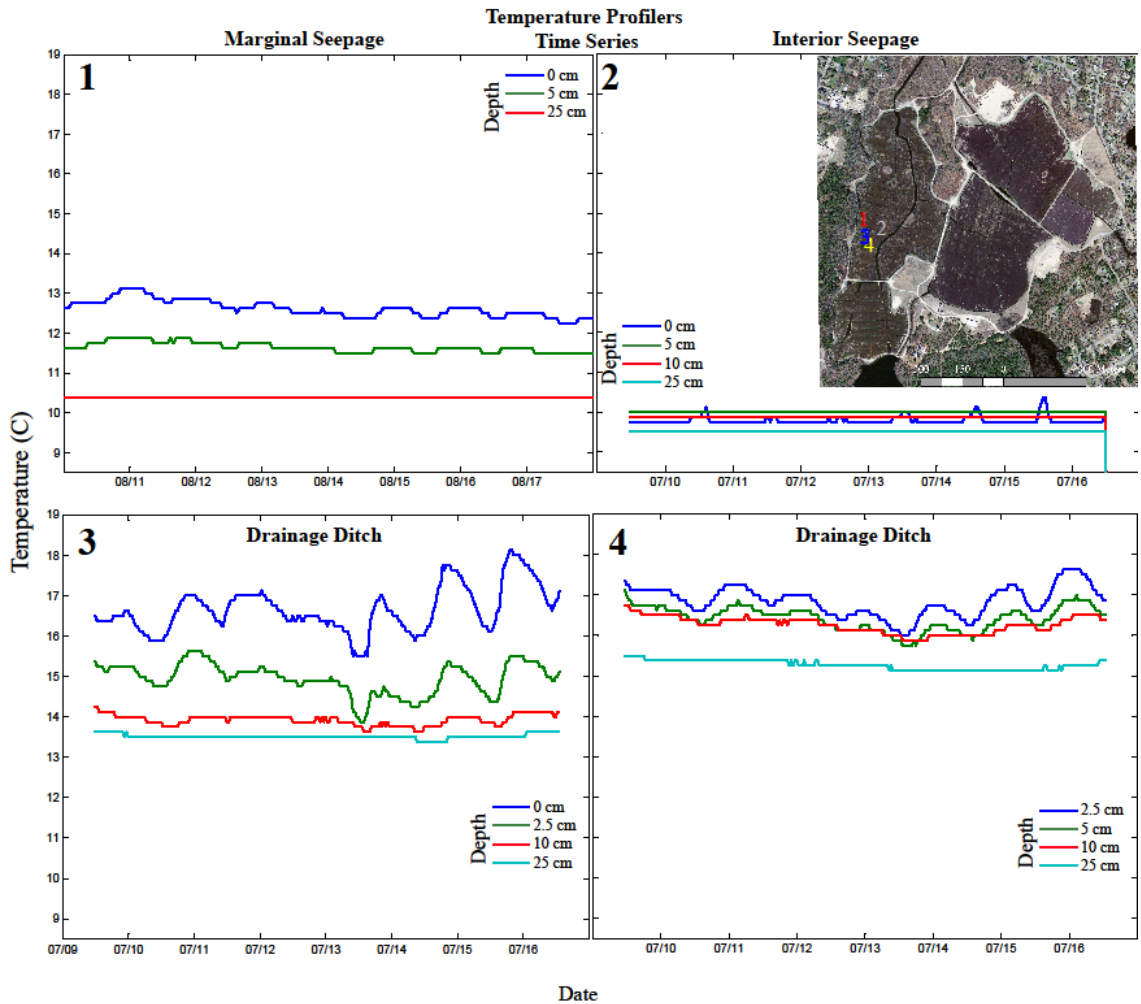
Figure 10: Time series of each thermistor from the thermal depth profiles installed within two types seepage zones and two surficial, ambient drainage ditches.

Although profile 4 has a thermal gradient with depth that is more linear than the other profiles it still indicates slight upwelling (slightly convex); which is affirmed through the 0.11 m d^{-1} flux calculations determined by the analytical solution. At -25cm both drainage ditch profiles converge on the local seasonal air temperature average; therefore potentially being more influenced by seasonal temperature signal reflected in

the pore waters rather than marginal seepage. *McKenzie et al.* (2007) observed that near-surface peat ($<$ 100 cm depth) in the summer emulates 0 cm air temperatures under little vertical flow conditions; as our profilers diurnal signal degrades by -25 cm depth the presence of an upwelling is probable.

4.3 Groundwater Sources

Stable water isotopes were compared from two identified large groundwater flow paths. One isotopic flow path signature was sampled from a deep groundwater well on the site, and the other was derived from data from USGS monitoring wells in the surrounding regional aquifer. These flow paths exhibit differing signatures as the on-site deep groundwater well isotopic signature was δO_{18} enriched in comparison to the δO_{18} depleted regional groundwater signature, presenting two end member signatures. This difference shows that the flow paths have unique source waters; the on-site deep well source was from a local lake, therefore it is referred to as the local groundwater flow path herein, and the others was sourced from up-gradient recharge, and is considered the regional flow path .

Water isotope samples were collected from on-site surface water, shallow groundwater wells, and thermally identified seepage locations. All seepage isotope samples were only collected once during September 2013, from 12 locations. All processed seepage samples exhibit an isotopic signature that more closely reflects the regional groundwater signature than the local groundwater signature (Figure 11). This indicates that the south-west regional flow path is the the large-field hydraulic gradient that forces the observed seepage patterns.

The east and west cell seepage are similar, as the eastern seepage results lay within the range of western cell seepage. The headwater seepage also lies within the range of western seepage. More seepage was identified within the western cells, hence more samples were collected and analyzed from the west. There are dissimilarities between the isotopic signatures from the collected western cells seepage. Six seepage samples trend away from the regional groundwater source and towards the local groundwater signature (Figure 11), and after further analyzes this is not due to any clear spatial differences (supplemental material). Within a δO_{18}/ δH_2 plot, any data trends that fall sharply to the right of the local meteoric line (more rapidly change δO_{18} than δH_2) may indicate evaporation. However, as the local groundwater source is an evaporative signature, the trending exhibited could be interpreted as a mixing line between the two flow paths. This signature may also reflect more interaction with the pore waters, or a difference in flux rates and/or flow path. The distinct seepage types had not been observed at the time of sampling, so more sampling would be necessary to analyze this further. This δO_{18} enrichment could also be a result of the surface sampling technique, as it would have been possible that the seepage was contaminated with more enriched surface water. The lack of spatial correlation would support the sampling surface water influence. However, these reasons are impossible to rule out within this dataset, and we are unable to make any clear interpretations of these enriched western cell seeps. All the remaining seeps, both east and west, show a depleted isotopic groundwater signature and therefore are assumed to be sourced from the regional groundwater. This means that a

southwest hydraulic gradient likely underlies the hydraulic development of all seepage zones within our site.

Western shallow groundwater isotope samples (from three wells) have isotopic signatures within the determined regional groundwater source, similar to the western seepage, but the groundwater wells do not show the enriched trending demonstrated in the western seepage. This observation supports that the seepage signature is more likely due to the sampling error than groundwater mixing. All shallow groundwater samples were sampled seasonally, and while there is little variability within the western samples, the eastern cell shallow groundwater samples (three wells) show large variability seasonally. We attribute this variability to the presence of the nearby southeast surface water bodies influencing the local groundwater signature. Locally we may expect a different groundwater flow path orientation as these southeastern ponds are not upgradient to the site on the regional hydraulic gradient, and for these eastern wells to exhibit such a distinct seasonality, an additional source would be needed for an explanation. In addition, the deep well signature that we use to describe the local groundwater source signature lies between the eastern peat cells and the southeast pond (Fresh Pond) (Figure 2), promoting this unique source mixing with regional groundwater. However, as mentioned above there are no thermally identified east seepage that exhibited an enriched δO_{18} signature; however as the summer shallow east groundwater values lie within the regional end member, and seepage samples were only taken in September it is not possible to conclude this singular source with confidence. The seasonality observed in the eastern shallow wells may be a product of a flow-reversal within the east cells, as seen at multiple

peatland sites (e.g. *Devito et al.*, 1997; *Fraser et al.*, 2001; *Reeve et al.*, 2006), but cannot

be constrained and is not discussed herein.
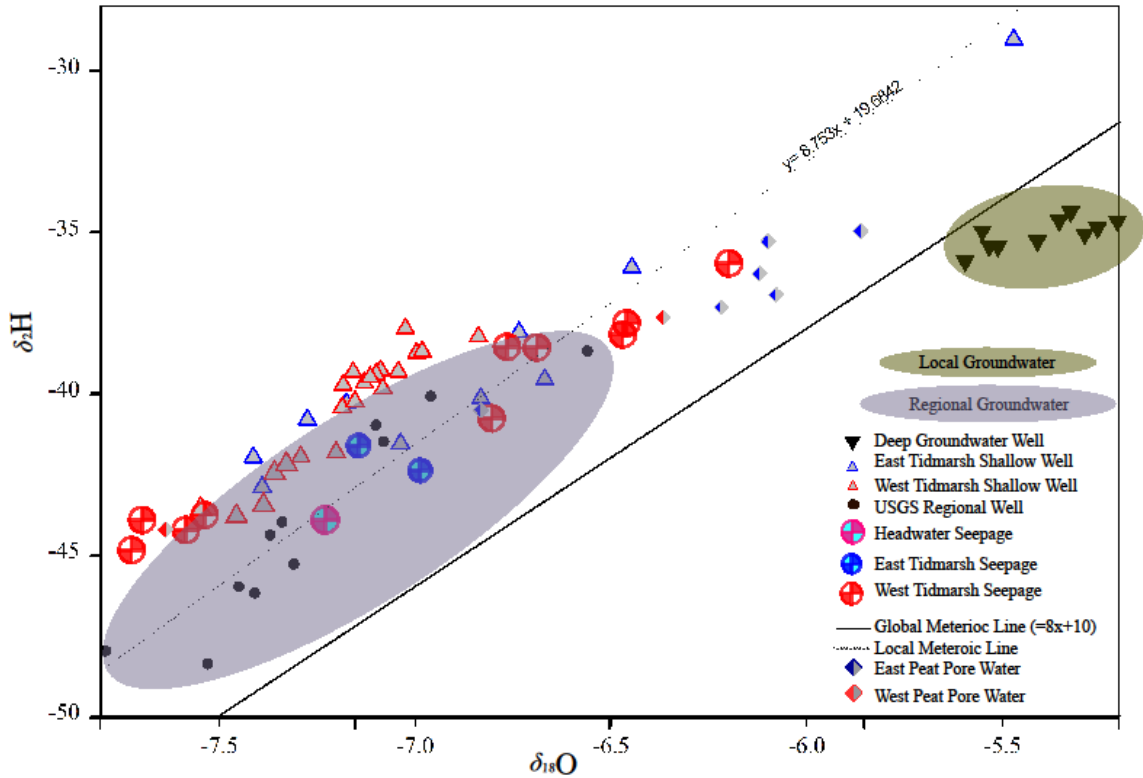
Figure 11: Stable isotope data indicating the potential ground water source. Seepage data that falls within the regional groundwater contour indicates that the northeast gradient is interacting with the subsurface to form these seeps. Seepage data that falls closer to the local groundwater contour indicates that these seepages were formed by north trending flow paths from local southern ponds.

Peat pore water samples were taken from 1 meter piezometers—one from the

eastern cells, and two western cells—and one hand core 1.3 meter deep in the eastern

cells. The two western peat pore waters show a wide variability between the samples;

one sample lies within the most depleted samples observed, and the other western sample

lies with the enriched samples, so no conclusions were drawn, and further fieldwork is

needed. The east peat pore waters show consistency more enriched δO_{18} signature, and none show a strong depleted signature. The pore water data that were collected from the eastern cells core were all highly enriched for our dataset, and did not exhibit a trend with depth.

Further comprehensive isotopic investigation will be necessary to distinguish the local and regional nature of the sources of these flow paths, and to better understand the hydrodynamics within the peatland matrix. The isotopic data are not able to fully elucidate the flow path story, however we are able to conclude that most seepage has a regional groundwater signature, and comes from the regional flow path direction. This reveals that the hydraulic forcing that interact with the peat basin and are responsible for inducing the groundwater discharge is from the southwest. This is important to understanding process-based development of peatland seepage, and their spatial distribution.

4.4 Hydrodynamic Data

4.4.1 Regional Hydraulic Head Gradient

The shallow groundwater well levels help evaluate local groundwater flow paths. Using the four wells that were installed along the margins we determined that the sand aquifer below Tidmarsh farms has a general horizontal hydraulic head gradient of 0.005 with a bearing of 010°. This interpretation is consistent with the large-scale regional aquifer flow maps generated by *Masterson et al.* (2009) and *Hansen and Lapham* (1998). This observation suggests that the most direct interaction with the regional hydraulic gradient would be at the southwest portion of the site, followed by the western edge (cell

3) while the eastern and northern cells are further down gradient. The southwest portion of the peat (cell 4) directly intersects with, and is the most perpendicular to, the regional flow gradient of the surrounding sand aquifer indicating high seepage potential; where regional flow in the sand aquifer meets low-hydraulic conductivity peat groundwater can be forced to the surface (discussed below). The groundwater discharge hypothesis presented by *Lowry et al.*, (2009) comments on the importance of the relative direction of hydraulic gradient with respect to the basal peat/aquifer interface when predicting seepage locations.

4.4.2 Groundwater well transects

Two well transects were installed on the western edge of the property, and were monitored for hydraulic head periodically during 2012-2014. The wells were installed at the edge of the peatland (marginal well- MW), and one at the strongest basal peat slope change, where interior seepage is predicted (interior well-IW) (Figure 2 shows their locations in map view, and Figure 3 shows a cross section of these transects). Only transect #1 (southern cell 3) was analyzed due to low sample frequency of the other transect. Along transect #1 the hydraulic head of the interior well was an average of 0.22 m (σ=0.008) greater than the marginal well (30 meters apart). This difference in head from the margin to the interior of the peat within the sand underlying the peat opposes the regional northeast hydraulic head gradient, as with these consistent head measurement a hydraulic gradient from the east to the west would be calculated. As the interior well is installed directly at the basin secondary slope break, the increase in head could be a localized effect. Additionally, the interior well is nested with a 1 meter well within the

59

peat to determine vertical hydraulic gradient at the basal peat slope change. The vertical gradient always remaining negative (upward flow) with a range from -0.01 to -0.06 ($\bar{x}$=0.044). The water level in the peat was very slow to respond to changes, which could have had an impact on the magnitude of the measurements, as it was difficult to purge.

4.4.3. Stream Flow Measurements

To determine how much stream water volume is being contributed through groundwater seepage we used differential gauging to determine stream flow at various distances along the mainstream channel, and major onsite tributaries. Differential gauging provides us with net channel gains/losses, however, due to the low K of peat, and previously run solute stream tracer experiment the channel was not expected to lose water; any gains can be attributed to groundwater seepage. On the east side (Cell 7) of the peatland the stream gained 6 L s^{-1} discharge from the Arm input to the confluence with Beaver Dam Brook (1.5 km), equal to an average of 0.004 L s^{-1} per meter of river length. The west side (Beaver Dam Brook - Cell 4 & 3) gained 113 L s^{-1} from the Beaver Dam Pond input to the confluence with East side river (1 km), equal to an average of

0.113 L s^{-1} per meter of river length. The greater input of water on the west side of the property reaffirms the temperature surveys, and supports the importance of the regional gradient orientation in groundwater discharge inputs.

CHAPTER 5

DISCUSSION

The basin structure under this groundwater-fed peatland influences the location and magnitude of groundwater seepage zones. Along the upgradient intersection of regional groundwater flow and the peatland margin there is a distinctive pattern of diffuse seepage, and in the peatland interior we observe discrete, stronger seeps as evidence by the presence of groundwater temperatures and thermal profiles. The interior seepage is caused by the orientation of the regional groundwater flow path in relation to the underlying peatland basin secondary slope; the reasons for these phenomena are discussed below.

5.1 Subsurface Structure control on Seepage Types

Within an aquatic peatland environment, groundwater seepage is defined as a location of low temperature standard deviation, and/or anomalous thermal signature. By this definition, two distinct types of groundwater seepage were observed: diffuse seepage, which occurs within 30 m of peatland margins, and discrete seepage, which occurs predominately in the interior of the peatland (> 10 m from the margin) (Figure 12). Both locations exhibit very similar standard deviation, but marginal seepage thermal anomalies has an average thermal signature 3-5 $^{\circ}$C offset from groundwater temperatures, while interior seepage exhibits a thermal signature comparable to groundwater temperatures. Marginal seepage is both warmer than expected groundwater temperature in the summer and colder than groundwater in the winter (Figure 4), illustrating the influence of

downward thermal conduction on seepage at these slower flowing diffuse upward seepage zones. The thermal variation between marginal and interior seepage is attributed to the mechanism of seepage zone development (diffuse flow vs. conduit flow) and the groundwater's residence time within the upper 100 cm of the peatland surface (thermally conductive horizon).

We observe many conduction-influenced marginal seeps within the first 30 m of the peatland edge (Figure 12), consistent with the marginal seepage observed in lake environments (*Sebestyen and Schneider*, 2004; *Rosenberry et al.*, 2010) and other wetlands (*Freeze*, 1988; *Labaugh et al.*, 1998). GPR and physical well data determine that the peat is 0-5 meters deep along this margin where seepage occurs (Figure 3), which is generally thinner than under interior discrete seepage locations. More seepage is observed at the shallowest part of the margin, and decreases rapidly with distance from the edge. This is consistent with the observed exponential decline in seepage presence from the initial landscape break within lakes (Figure 12) (*Cherkauer and Zager*, 1989). This lower K peat intercepts the water table inducing a difference in hydraulic head from the surface to the aquifer, resulting in an upward flux generating the observed marginal seepage. As proposed by *Winter* (2001), the initial slope change within the basin structure causes seepage to occur along the edge of the wetland, comparable to lake seepage. Figure 13 provides a conceptual model of this process. This similar seepage develop process is observed in riverine systems (*Campana et al.*, 1994), lake (*Winter*, 1976; *Genereux and Bandopadhyay*, 2001) and hillslope environments ((*Dunne and Black*, 1970; *Sophocleous*, 2002).
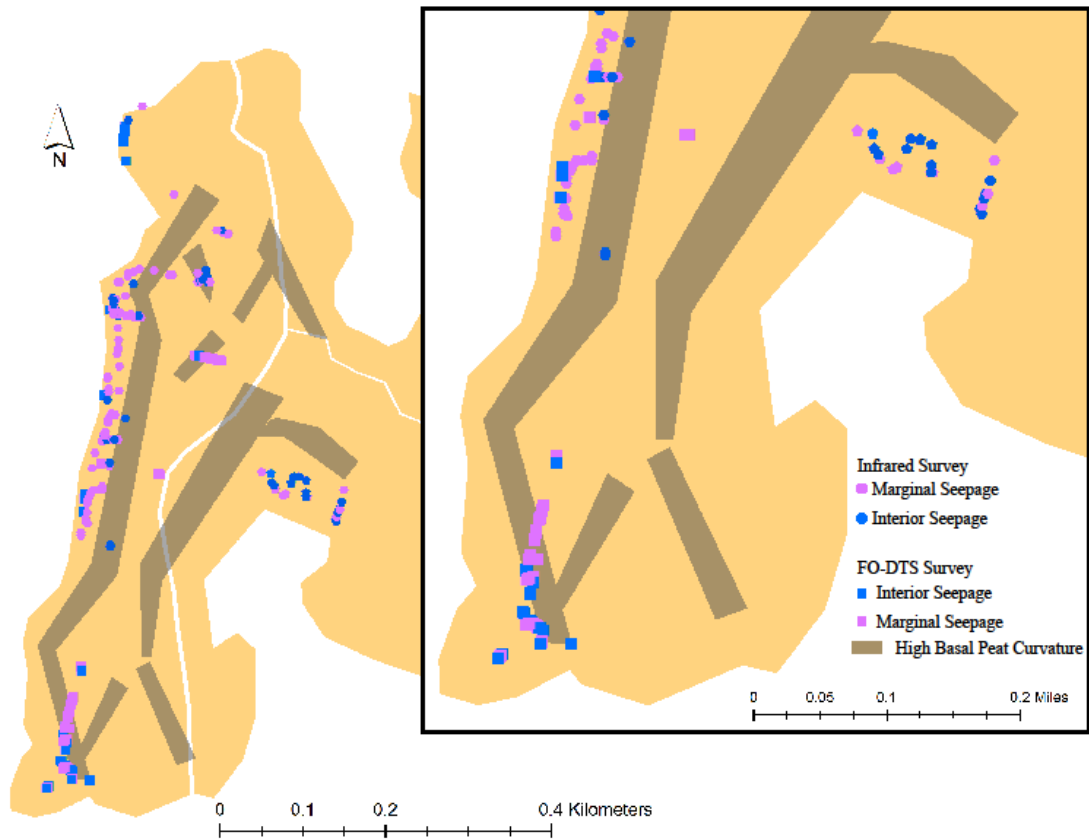
Figure 12: Locations of seepage determined by both infrared and FO-DTS surveys. Interior seepage is defined as groundwater temperature and standard deviation lower than 1.5. Marginal seepage has a temperature 3-5 C closer to air temperature than groundwater. High basal curvature locations were generalized from figure 3.

In contrast to the diffuse marginal seepage, interior seepage was less common and was spatially disconnected from similar seeps (Figure 12). Interior seepage exhibits low standard deviation of temperature, similar to marginal seepage (Figure 5); however, at interior seeps groundwater temperature are observed, which indicates little surface diurnal conduction downward, indicative of strong vertical up advection (Figure 9 & 10). These locations are likely associated with the "peat piping" or macropore development explored in other peatland literature (e.g. *Jones*, 2010; *Wallage and Holden*, 2011; *Smart*

et al., 2012; *Cunliffe et al.*, 2013).   In both the continuous FO-DTS measurements and the discrete infrared images, these seepage areas have temperatures that are similar to groundwater.   Therefore, there is a low residence time (fast upwelling flux) through the peat's thermal conductive zone of the upwelling groundwater. This observation suggests preferential pathway flow, and strong advective flux rates, both which are supported by visual evidence of macropores at several interior seepage locations (e.g. Figure 9). The vertical temperature profile results support surficial temperature observations, as there is very little change in the thermal signature at the surface. This demonstrates that the upward advective rate in strong enough to limit the downward propagating surface temperature conduction signal, and therefore indicates an upward flux of greater than that of the marginal seepage.

These interior seepage zones, with indicated strong, preferential flow, are located above significant basal peat slope change, or high curvature, as hypothesized by *Lowry et al.* (2009) and *Rossi et al.* (2012). This change is caused by the strong discontinuity in hydraulic conductivity promoting a transition from horizontal flow to vertical flow. The peat is thicker in the interior of the peatland than along the marginal seepage zones (Figure 3) increasing the flow path length from the aquifer sand below to the surface of the peat. Yet the thermal signature of the groundwater is altered less through this longer distance travelled through the peat, than the short flow length marginal seeps. The lack of observed surface conduction influence on interior seepage temperatures indicate fast advection and short residence time even with this increased flow path length, particularly within the upper horizon of the peatland surface. The increased fluid flux in comparison
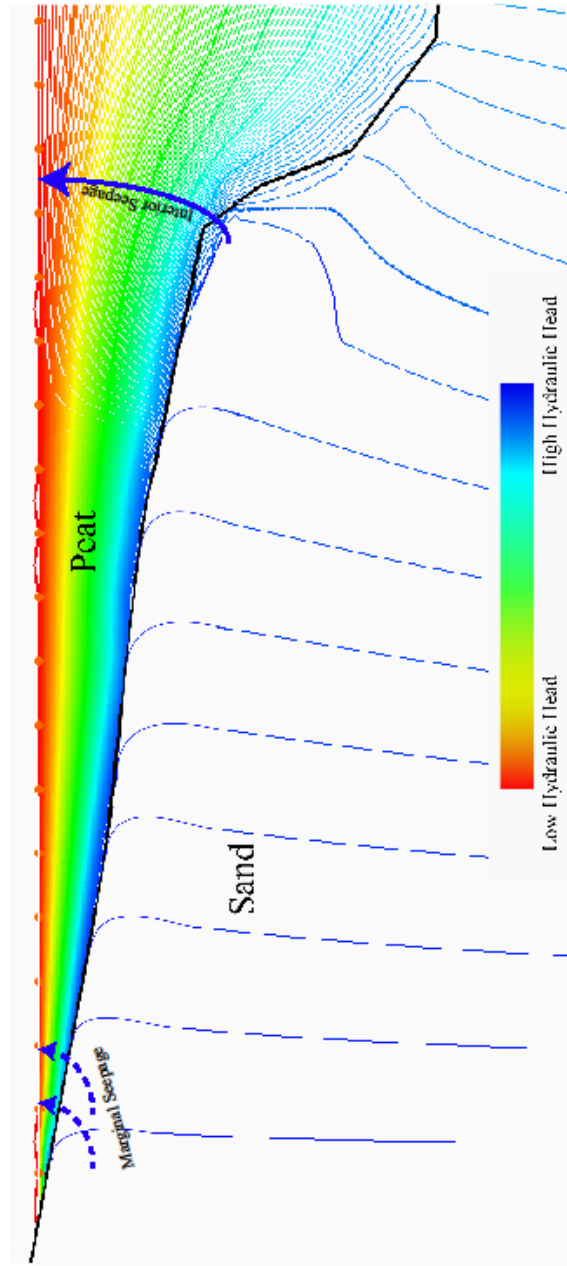
Figure 13: Conceptual cross-section of the subsurface peat hydraulic head distribution. There is a slight increase in hydraulic head where the underlying sand aquifer contacts the steep slope peat. This increase in pressure, in combination with localized high effective K, induces high seepage rates within the interior of the peatland. Marginal seepage are seen along the edge of the peatland where there is the initial decrease in K, and the peat is much thinner

to diffuse marginal seeps requires both an increase in vertical hydraulic gradient through the peat, and an increase in effective hydraulic conductivity specific to the seepage locations, greater than expected for thick peat sequences. The increased hydraulic gradient is due to the secondary slope break (interior from the margin) of the peatland basin, when it is perpendicular to the regional flow gradient of the aquifer (Figure 13). While the stark change to low hydraulic conductivity has long been known to promote the transition from horizontal to vertical flow (*Freeze and Witherspoon*, 1967), Lowry et al. (2009) was first to recognize how this process developed seepage within the interior of a peatland through development of a 3D groundwater flow model. As regional water is forced to go through or around the low-conductivity peatland, pressure is increased by the abrupt change in the hydraulic conductivity from the sand to catotelm peat matrix. At well transect #1 (Figure 1- MW1 & IW1) we observe an anomalous increase in hydraulic head at the wells installed on the subsurface slope change, in comparison to the wells closer to the edge of peatland. This observation opposes the direction of the regional aquifer gradient, and establishes the presence of a higher localized hydraulic head at this location of high basin curvature within peat basin structure.

The differences in the thermal profiles between profiler locations result from changes to the magnitude of flux consistent with the lower-flux, diffuse marginal seepage and higher-flux, focused interior seepage. This change in flux magnitudes are caused by subsurface hydraulic gradient shifts and effective hydraulic conductivity changes. Marginal seepage maintains a flux of 0.23 m d^{-1}, while temperature profile data (Figure 9 & 10) determines that the interior seepage much higher flux rate outside the sensitivity

limits of the steady-state analytical method, which (*Conant Jr.*, 2004) indicates could be as high as -1440 m d^{-1}.

The surface temperatures of the ambient drainage ditches, determined with the FO-DTS, closely relates to the diurnal temperature cycles. As most ditches' stages were low (<0.5m) and had no thermally significant influx of groundwater, they would experience temperatures similar to air temperature (Figure 5). However, the subsurface profiler results (n=2) still show a characteristic upwelling thermal envelope (convex shape); except the envelope is transformed laterally, exhibiting temperatures 5 °C warmer than the marginal seepage profiles (7-10 °C warmer than groundwater temperature). In addition, these depth-temperature profiles converge on 14-15 °C at -25 cm, significantly warmer than the groundwater temperature. The 1D flux solutions were -0.11 and -0.20 m d^{-1} for these same drainage ditches, which are very comparable to the observed marginal seepage flux (-0.23 m d^{-1}). Therefore, while these locations were installed to act as expected control points and determine pure-conduction values, upwelling was observed. A longer flow path within the peat's conductive horizon may explain the similar vertical flux rates to marginal seepage, but a warmer surface expression. The inability for our surface temperature tracer methods to identify these locations as sources of upwelling illustrates that monitoring surface temperature alone can miss seepage influx when there is little temperature contrast, which may be important in the water balance to the site. The FO-DTS did indicate some of these seepage zones as locations of low standard deviation of temperature, but our criteria of average temperature near groundwater would have to be reassessed to account for these seepage, as they are much warmer than groundwater (Figure 6). As the scope of this paper has been to describe locations of groundwater

seepage and seepage patterning to better design peatland restorations focusing on the inclusion of cold-water thermal refugia, warm seepage patterning and development is not a focus. These seepage do not provide thermal buffering that is required of many thermally stressed aquatic species. However, finding all surface seepage zones will be important when further developing a process-based understanding of peatland hydrodynamics.

5.2 Seepage groundwater sources

Understanding the hydraulic gradients and subsequent flow paths surrounding a peatland are central to developing process-based predictions of seepage zone formation. The groundwater isotopic signature of all the sampled seepage locations are similar to the regional groundwater source, but some seepage to exhibit surface water/local flow path mixing (Figure 11). Therefore, the regional gradient is responsible for the pressure shifts causing the seepage locations, but it may be a result of both deep and shallow flow paths. *Cheng and Anderson* (1994) predicted that both shallow and deep groundwater additions are important to monitor in lakes within regional groundwater discharge areas. The orientation of peatland basin slope break and the regional groundwater gradient dictates the observed pattern of seepage distribution, and relative dominance on the site. Due to the strong regional gradient at this site, our conceptual model best applies to groundwater-fed peatlands with significant regional gradients, typical of coastal peatlands.

In areas where local flow paths may have a higher magnitude gradient in comparison to the regional gradients, such as continental interiors, we would expect local

recharge and flow paths to control the zones of seepage. These local flow paths are typically more sensitive to climatic and seasonal changes in evaporation and precipitation (*Fraser et al.*, 2001; *Reeve et al.*, 2006). Observed reversals in hydraulic gradients have been common (*Siegel et al.*, 1995; *Devito et al.*, 1997; *Reeve et al.*, 2006), which likely will play a role in seepage development and persistence in local-flow dominated environments. Therefore, more prolific sampling needs to be completed to more concretely understand the nature of the flow paths beneath the this type of peatland.

5.3 Development of seepage patterns

The spatial seepage distribution observed at the Tidmarsh peatland draws parallels to lake environments allowing for insight into the development of peatland seeps through time. As kettle hole peatlands typically form from initially open water bodies, observed similarities between the two environments are logical.

Marginal seepage extends beyond the edge of the peatland (Figure 12), and are observed until the interior slope change. These seepage zones may also exhibit higher effective K, which could be explained littoral-zone migration in the preceding lake/wetland due to water table fluctuations. In lake environments, diffuse marginal seepage occurs because of an increase in hydraulic conductivity at the edge of the lake caused by erosional deposition, increased wave break and current disruption, and the concentration of flow paths from the break in land surface slope (*McBride and Pfannkuch*, 1975; *Winter*, 1976, 2001; *Cherkauer and McKereghan*, 1991; *Rosenberry et al.*, 2010; *Blume et al.*, 2013). *Cherkauer and Zager* (1989) propose that seepage flux decreases exponentially with distance from shore within a lake, which is qualitatively

confirmed by our data. Paleoclimate reconstructions have demonstrated that the regional water table around Tidmarsh has been predominately increasing in elevation since the Laurentide ice sheet retreated ~ 10 ka ago, with 2-3 significant low stands (*Newby et al.*, 2000, 2009). Therefore, we hypothesize that the extent of the marginal seepage seen along the western edge of the peatland is a result of this transgression and a decrease in the stability of peat deposition.

Interior seepage develops at locations of distinct hydraulic conductivity change from the sand aquifer to the peat matrix coincident with a zone of anomalously high hydraulic pressure caused by the intersection of regional groundwater flow and high basal curvature zones (Figure 12). When the regional flow lines slow abruptly due to this change in matrix, pressure builds at the interface and induces a vertical gradient, causing the observed relationship between dramatic basal peat slope changes (high curvature) and the observed strong upward fluxes. In addition, there is little lateral flow that can develop through accumulated catotelm (*Belyea and Clymo*, 2001) and potential lacustrine sediments that have accumulated within the deeper portions of the lake. The strong advective seepage flux is potentially greater than that at the more diffuse, marginal seepage because of the more localized, greater slope change/curvature at the interface of the lower hydraulic conductivity peat (Figure 10). Discrete seepage at secondary slope changes are observed in lake environments (*Genereux and Bandopadhyay*, 2001), but are less common as there is a less of a dramatic change in hydraulic conductivity properties, no "semi-confinement" of the aquifer, and also likely due to the difficultly in sampling seepage in deeper waters.

70

Rosenberry (2010) notes that in lakes a significant upward seepage velocity can maintain a locally high hydraulic conductivity as the upward force may suspend smaller particles within the water column. Particulate organic matter and lacustrine sediment have a very low settling velocity, therefore if the upward force that groundwater seepage induces is greater than the settling velocity, only organic matter with a high mass will be able to accumulate over these lake seepage locations. This would cause the peat matrix to have a relatively high porosity, high permeability zones compared to its surrounding very low permeability matrix. These locations will continue to be zones of weakness through the formation of the peatland, and is likely why there is a strong relationship between original kettle lake seepage locations and discrete seepage zones observed in peatlands.

We propose is that high-flux interior seepage zones persist through the transition from lake to peatland environment due to the inability of fine sediments and organic matter to accumulate over these high flux locations. Still, these consistent high pressure locations will also continually take advantage of inherent matrix weaknesses, such as varying degrees of humification caused by vegetative difference and water level, or other disruptions in the peat matrix including plant rooting and desiccation 'cracks' as proposed by *Smart et al.* (2012). However, the underlying mechanics of interior seepage are caused by the subsurface structure interacting with the regional gradients.

CHAPTER 6

CONCLUSION

Subsurface basin shape exhibits significant control on the spatial distribution of groundwater seepage within peatland environments. As horizontal groundwater flow intercepts the peat matrix, two types of seepage develop: marginal and interior seepage. Marginal seepage is defined by a low standard deviation in temperature and surface temperature 3 -5 $^{\circ}$C different from groundwater, indicating low-flux seepage. This low flux is attributed to the regional flow paths intercepting the low-K peat land at the initial basin 'shoreline' inducing upward flow through peat 0.1- 3.0 meters thick. Interior seepage, the second type of seepage, has a surface temperature expression indistinguishable from groundwater temperature. This indicates a strong upwelling flux at these locations. Interior seepage locations correlate with high rates of slope change (or curvature) within the peat basin. These seeps develop where the regional flow path intercepts the secondary slope change and where there is a stark change in hydraulic conductivity between the high-K sand aquifer material and the low-K peat. These physical features together induce localized zones of high vertical gradient, supplying seepage flux. As interior seeps occur through much deeper peat they must have a much higher vertical hydraulic gradient than the marginal seeps to maintain groundwater temperatures. Through multiple lines of evidence, we conclude that the process of mineraltropic peatland seepage development and spatial distribution is strongly controlled by the interaction between the subsurface basin structure and the hydraulic gradient.

Through our results, we have established a predictable pattern of seepage, consistent across the coastal site that is explained by knowledge of the basin shape and the regional hydraulic gradient. This information provides valuable insight for water resource managers to understand the natural forces driving groundwater seepage, which is a highly desired ecosystem process notably for thermally stressed species. Knowledge of where seepage is expected to occur naturally will allow for a more sustainable, process-based restoration design by encouraging groundwater inputs in low-gradient systems through a focused restoration effort. Already this approach has been utilized in the restoration design for this degraded peatland. The resource managers plan to build the new sinuous stream along the locations of high basin curvature to induce groundwater seepage to the main channel. The goal of this is promote a healthy, thermally buffered main channel to encourage biodiversity and the return of anadromous fish species. This knowledge is transferable to other coastal sites as well. With the process-based knowledge of the physical seepage controls, seepage distribution can be predicted with just groundwater wells, to establish the regional gradient, and a geophysical survey. Incorporating this data into a restoration design will greatly aid the ability to predict and achieve desired ecosystem outcomes, making restoration project more efficient, both ecologically and monetary.

This research has provided a much-needed illumination of the subsurface hydrodynamics within a peatland. While a peat matrix exhibit strongly heterogeneous and anisotropic tendencies, large-scale patterns occur and can be predicted. These patterns are dependent on the shape of the basin, peat accumulation history, and the aquifer flow paths below. The importance of the aquifer flow paths surrounding the peatland to

seepage patterns emphasizes that peatlands are not isolated entities from the groundwater system and cannot be treated as such. This observed large-scale seepage patterning provides insight that may help explain vegetation patterning, macropore development, and other localized peat dynamics that have been unidentified in the past, and greatly aid peatland management and restoration to establish more naturally sustainable, efficient practices.

A.1 STABLE WATER ISOTOPES

Full δ_{18}O and δ_2H isotopic data set recorded from August 2012-March 2014.

Shallow Wells

Date	Sample ID	Depth (m)	δ_{18}O	δ_2H	Location	Season	Well Cluster
9/16/12	IF5A	2.41	-6.7584	-38.7151	South	Fall	Transect 4
9/16/12	IF5B	1.01	-6.8994	-39.2429	South	Fall	Transect 4
11/12/12	IF5A	2.41	-6.9168	-39.3757	South	Fall	Transect 4
11/12/12	IF5B	1.01	-6.9635	-39.6393	South	Fall	Transect 4
11/12/12	TM5a.2	2.95	-7.2131	-41.9111	West	Fall	Transect 1
11/23/12	TM1.D	2.45	-5.3472	-35.4452	East	Fall	Transect 3
11/23/12	TM5a.1	1.00	-7.3593	-43.4152	West	Winter	Transect 1
12/16/12	IF5B	1.01	-7.0463	-39.7023	South	Winter	Transect 4
12/16/12	Barn	9.00	-6.5055	-40.1152	Well	Winter	Residential Well
12/16/12	DJ	12.8	-5.9117	-36.0751	Well	Winter	Residential Well
1/20/13	IF5A	2.41	-6.8902	-39.8135	South	Winter	Transect 4
1/20/13	IF5B	1.01	-7.0079	-39.3062	South	Winter	Transect 4
1/20/13	Barn	9.00	-6.2545	-39.5276	Well	Winter	Residential Well
1/20/13	TM5a.1	1.00	-7.6067	-43.542	West	Winter	Transect 1
2/3/13	TM5a.2	2.95	-7.2699	-42.1531	West	Winter	Transect 1
2/23/13	IF5A	2.41	-6.8018	-37.96	South	Winter	Transect 4
2/23/13	IF5B	1.01	-6.9406	-39.46	South	Winter	Transect 4
3/17/13	IF5A	2.41	-7.3649	-42.85	South	Spring	Transect 4
3/17/13	IF5B	1.01	-7.0331	-40.27	South	Spring	Transect 4
4/6/13	TM5a.1	1.00	-7.4658	-43.76	West	Spring	Transect 1
4/6/13	TM5a.2	2.95	-7.3162	-42.42	West	Spring	Transect 1
5/24/13	IF5A	2.41	-7.1871	-40.7706	South	Spring	Transect 4
5/24/13	IF5B	1.01	-7.3997	-41.9321	South	Spring	Transect 4
7/11/13	IF5A	2.41	-7.05	-40.39	South	Summer	Transect 4
7/11/13	IF5B	1.01	-7	-40.21	South	Summer	Transect 4

7/29/13	IF5A	2.41	-6.736	-38.6773	South	Summer	Transect 4
7/29/13	IF5B	1.01	-7.0736	-41.7727	South	Summer	Transect 4
7/29/13	DJ	12.8	-6.3554	-38.0702	Well	Summer	Residential Well
8/1/13	Barn	9.00	-6.821	-41.5115	Well	Summer	Residential Well
8/7/13	TM1.D	2.45	-4.4118	-29.0261	East	Summer	Transect 1
8/16/13	IF5A	2.41	-6.8301	-39.2904	South	Summer	Transect 4
8/16/13	IF5B	1.01	-6.5152	-38.2084	South	Summer	Transect 4
9/14/13	TM1.D	2.45	-4.5863	-29.1158	East	Fall	Transect 3

Groundwater Seepage

Date	Location	$\delta_{18}O$	δ_2H	Cell
4/6/2013	West	-6.8048	-40.7829	Cell 4
4/6/2013	West	-6.1986	-35.9783	Cell 3
8/1/2013	West	-6.6893	-38.5886	Cell 3
8/1/2013	West	-7.5376	-43.78	Cell 3
8/1/2013	West	-7.5856	-44.24	Cell 3
8/1/2013	West	-6.4602	-37.8355	Cell 4
9/14/2013	West	-6.4696	-38.1826	Cell 4
9/14/2013	West	-6.7655	-38.568	Cell 4
9/14/2013	West	-7.6973	-43.9302	Cell 4
9/14/2013	West	-7.724	-44.8669	Cell 4
9/14/2013	West	-7.2297	-43.928	Cell 5
9/14/2013	East	-6.9875	-42.3947	Cell 6
9/14/2013	East	-7.1446	-41.6296	Cell 6

Surface Waters

Date	Sample ID	$\delta_{18}O$	δ_2H
7/11/2012	BDPO	-6.90	-41.14
7/11/2012	FPC	-6.79	-40.47
7/11/2012	IF2	-6.83	-41.71
7/11/2012	IF3	-7.07	-41.85
7/11/2012	IF4	-6.79	-41.51
7/11/2012	IF7	-6.12	-37.93
7/11/2012	Arm	-6.13	-37.78
8/17/2012	BDPO	-6.81	-41.87
8/17/2012	FPC	-6.49	-38.56
8/17/2012	IF2	-5.33	-37.69
8/17/2012	IF3	-6.744	-40.3472
8/17/2012	IF4	-6.7785	-40.379
8/17/2012	IF7	-6.0488	-36.5461
9/15/2012	FPC	-3.5222	-26.0614
9/15/2012	IF2	-6.9431	-41.3455
9/15/2012	IF3	-6.8549	-41.3468
9/15/2012	IF4	-6.8444	-41.4864
9/15/2012	IF7	-6.0037	-37.5727
9/16/2012	BDPO	-6.6163	-40.6145
9/16/2012	Arm	-2.1283	-20.1901
9/29/2012	BDPO	-6.5932	-38.832
9/29/2012	IF2	-6.9379	-40.579
9/29/2012	IF3	-7.1321	-41.4745
9/29/2012	IF4	-6.9109	-41.6842
9/29/2012	IF7	-6.1618	-36.8856
9/30/2012	BDPO	-6.8011	-41.1219
9/30/2012	FPC	-7.7888	-51.8166
9/30/2012	Arm	-3.031	-23.8713
11/12/2012	BDPO	-6.8966	-40.9377
11/12/2012	FPC	-6.4287	-38.1214
11/12/2012	IF2	-7.0007	-41.4355
11/12/2012	IF3	-7.0505	-41.3006
11/12/2012	IF4	-6.9065	-41.3434
11/12/2012	IF7	-6.2993	-37.9088
11/12/2012	Arm	-4.4827	-29.7179

11/23/2012	Little Island Pond	-6.9395	-39.608
12/16/2012	BDPO	-6.708	-40.6096
12/16/2012	IF2	-6.8374	-41.6287
12/16/2012	BDPO	-6.7685	-40.5908
1/20/2013	BDPO	-6.6155	-40.88
1/20/2013	IF3	-6.9228	-41.2136
2/23/2013	BDPO	-6.4413	-41.16
2/23/2013	FPC	-2.8343	-22.02
2/23/2013	IF2	-6.654	-40.26
2/23/2013	IF3	-7.2433	-43.26
2/23/2013	IF4	-7.4283	-44.13
2/23/2013	IF7	-4.5774	-30.55
3/17/2013	BDPO	-6.8089	-41.33
3/17/2013	FPC	-3.4835	-25.95
3/17/2013	IF2	-6.8898	-41.25
3/17/2013	IF3	-7.2233	-43.09
3/17/2013	IF4	-7.5184	-44.45
3/17/2013	IF7	-4.577	-30.62
5/24/2013	BDPO	-6.6267	-40.7524
5/24/2013	FPC	-3.079	-23.5795
5/24/2013	IF2	-6.7799	-40.9289
5/24/2013	IF3	-6.7447	-40.7117
5/24/2013	IF4	-7.5402	-44.1087
5/24/2013	IF7	-5.3449	-34.8038
5/24/2013	Arm	-3.8281	-29.2239
7/6/2013	IF4	-6.7135	-41.3224
7/6/2013	IF3	-6.1581	-36.0433
7/6/2013	BDPO	-5.9085	-34.8361
7/16/2013	FPC	-2.7986	-21.9111
7/16/2013	IF2	-6.7767	-41.0645
7/16/2013	Arm	-4.2664	-28.0259
7/19/2013	IF2	-6.3574	-36.8263
7/29/2013	BDPO	-6.8248	-40.6571
7/29/2013	FPC	-2.6602	-21.5705
7/29/2013	IF3	-7.1646	-42.8341
7/29/2013	IF4	-7.2314	-42.6866
7/29/2013	IF7	-6.1924	-38.5007
7/29/2013	Arm	-5.6337	-35.3566
9/14/2013	BDPO	-5.7548	-35.152
9/14/2013	IP7	-5.2862	-32.5163
9/14/2013	IP4	-6.1851	-36.3678

9/14/2013	Arm	-5.4229	-32.5552
9/14/2013	IF3	-6.016	-35.3094
9/14/2013	IF2	-6.074	-35.4101

Peat Pore Waters

Date	Sample Location	Depth (cm)	$\delta_{18}O$	δ_2H
10/6/2013	Cell 7	63	-6.1206	-36.29
10/6/2013	Cell7	55	-6.0987	-35.30
10/6/2013	Cell 7	105	-6.0783	-36.95
10/6/2013	Cell3	100	-6.3658	-37.66
10/6/2013	Cell 7	105	-6.2182	-37.34
9/14/2013	Cell 7	100	-5.8619	-34.98
2/3/2013	Cell 3	100	-7.6373	-44.23
11/23/2013	Cell 2	100	-6.8319	-40.53

Precipitation

Date	Type	$\delta_{18}O$	δ_2H
9/29/2012	Rain	-3.214	-19.53
9/30/2012	Rain	-9.6604	-63.25
2/12/2013	Rain	-2.4543	-16.00
2/12/2013	Rain	-2.448	-16.22
2/12/2013	Rain	-2.493	-15.68
2/12/2013	Rain	-3.0745	-12.95
7/1/2013	Rain	-2.7993	-12.96
7/1/2013	Rain	-2.7252	-12.45
7/1/2013	Rain	-2.6325	-12.42
7/13/2013	Rain	-3.0175	-18.02
7/23/2013	Rain	-8.523	-57.66
7/23/2013	Rain	-9.7151	-63.70
7/11/2013	Rain	-4.3338	-20.15

Deep Groundwater

Date	Location	Depth (m)	$\delta_{18}O$	δ_2H
7/11/2012	Guest House Well	12.3	-5.29	-35.07
8/17/2012	Guest House Well	12.3	-5.5514	-34.98

9/15/2012	Guest House Well	12.3	-5.2063	-34.67
9/30/2012	Guest House Well	12.3	-5.3263	-34.39
11/12/2012	Guest House Well	12.3	-5.3548	-34.66
12/16/2012	Guest House Well	12.3	-5.4107	-35.28
1/20/2013	Guest House Well	12.3	-5.1453	-34.57
1/20/2013	Guest House Well	12.3	-5.5339	-35.44
3/17/2013	Guest House Well	12.3	-5.5952	-35.92
5/24/2013	Guest House Well	12.3	-5.2574	-34.89
7/29/2013	Guest House Well	12.3	-5.5115	-35.46
9/14/2013	Guest House Well	12.3	-4.4311	-28.80

USGS Plymouth-Carver-Duxbury-Kingston Aquifer

County	Date	USGS: station ID	Depth (m)	$\delta_{18}O$	δ_2H
PLYMOUTH	7/25/2001	414604070381402	18.1	-7.34	-44
PLYMOUTH	10/12/2000	415012070461101	91.4	-7.53	-48.4
PLYMOUTH	8/11/1999	415317070434701	4.3	-7.45	-46
PLYMOUTH	8/11/1999	415423070442901	9.1	-8.03	-50
PLYMOUTH	8/4/1999	415541070443001	13.1	-7.41	-46.2
PLYMOUTH	9/1/1999	420044070430301	12.2	-8.04	-50.4
PLYMOUTH	8/31/1999	420134070432301	7.6	-7.08	-41.5
PLYMOUTH	8/25/1999	420144070541501	6.1	-7.37	-44.4
PLYMOUTH	7/29/1999	420239070472201	7.0	-8.08	-51.2
PLYMOUTH	9/2/1999	420249071035801	5.5	-7.79	-48
PLYMOUTH	8/25/1999	420607070515501	2.4	-7.1	-41
PLYMOUTH	8/23/1999	420634070444201	12.2	-7.31	-45.3
PLYMOUTH	8/24/1999	420910070530901	4.6	-6.56	-38.7
PLYMOUTH	8/24/1999	420937070513001	4.6	-8.04	-49.3

U.S. Geological Survey, 2013, National Water Information System data available on the World Wide Web (Water Data for the Nation), accessed [September 1, 2013], at URL [http://waterdata.usgs.gov/nwis/].

A.2 AIR TEMPERATURE AND PRECIPITATION OVER FO-DTS DEPLOYMENTS

Maximum and minimum recorded air temperatures and precipitation amounts over the FO-DTS deployments (June-August 2013). Data recorded at Plymouth Municipal Airport.
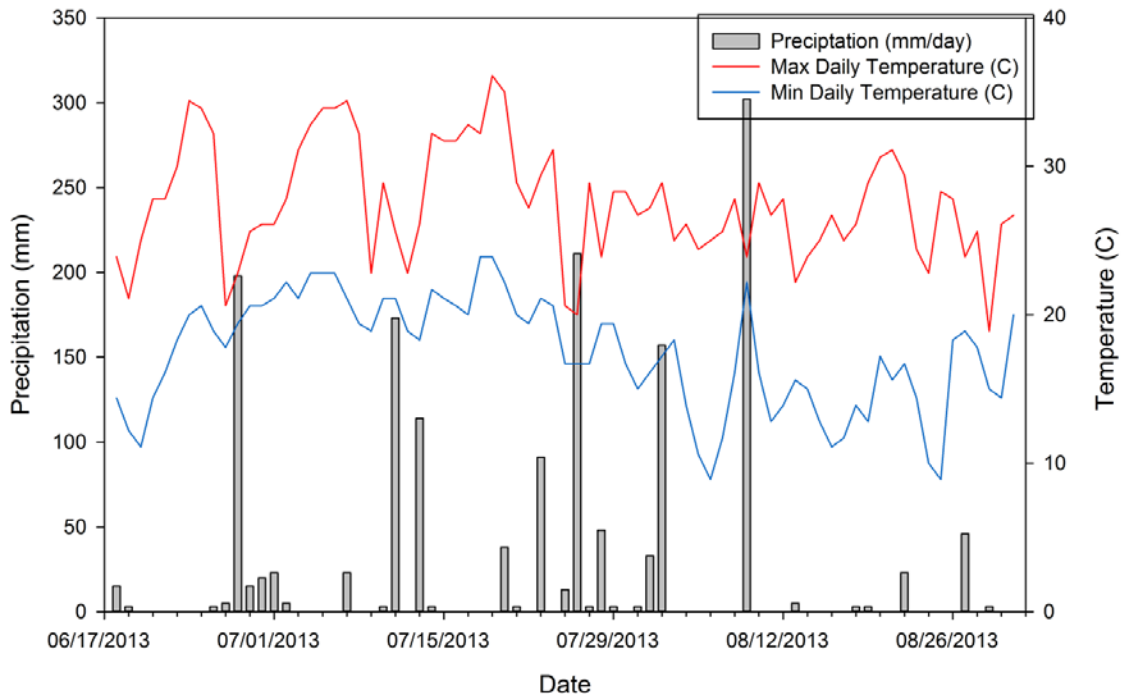
National Ocean and Atmospheric Administration, 2013, National Climatic Data Centre data available on the World Wide Web (Water Data for the Nation), accessed [October 1, 2013], at URL [http://www.ncdc.noaa.gov/data-access]
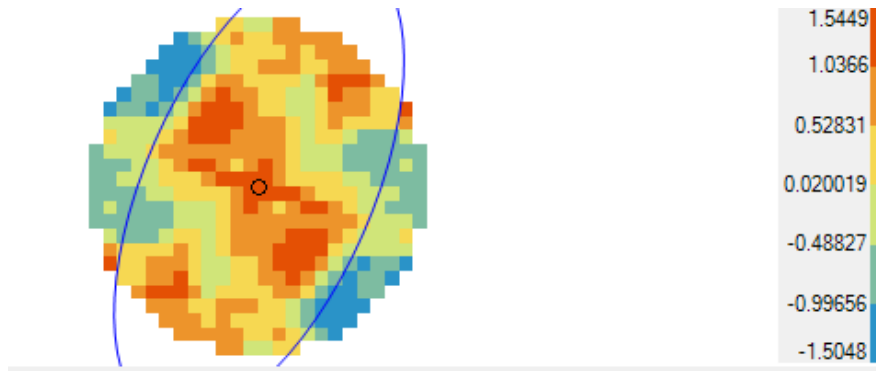
A.3 GEOSTATISTICAL VARIOGRAM

Kriging variogram used to generate peat thickness maps by interpolating ground penetrating radar point data.

Variogram
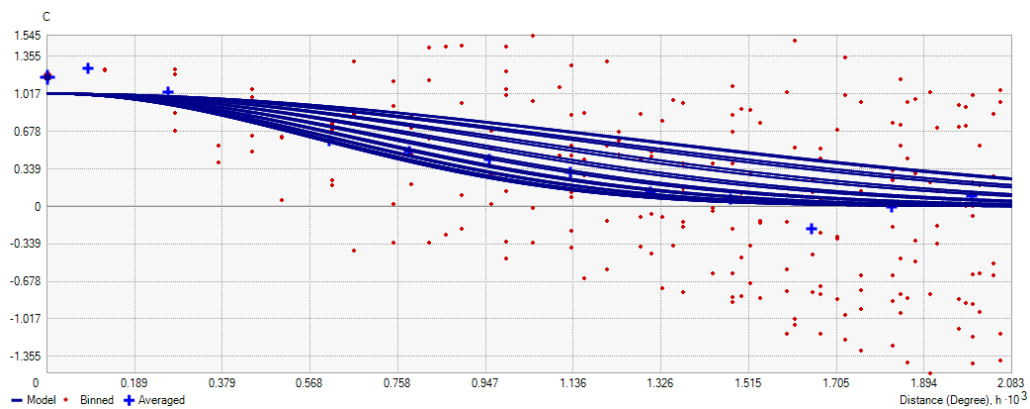
Covariance Map

A.4 HYDRAULIC HEAD MEASURES

Hand measured hydraulic head measurement in meters above sea level from site wells over 2 years.

Date	Metal	Plastic (Shallow)	5a.1 (West)	5a.2 (East)	5a.3 (Peat)	1.1 (deep)	1.2(peat)
14-Apr-12	4.151	3.800					
9-Jul-12	4.122	3.712					
30-Aug-12	4.091	3.650					
7-Oct-12			2.880	2.930	2.870	2.500	2.160
22-Nov-12						2.500	2.000
3-Feb-13	3.261	3.380	2.755	2.845	2.865		
6-Apr-13			2.845	2.860	2.828		
7-Jul-13			2.892	2.955	2.836		
7-Aug-13			2.883	2.939	2.808		
14-Sep-13						2.534	2.510

Well hydraulic head measurements from western wells. Blue line is data from a well located on a basin slope change, while the light pink line is data from a marginal well on the same transect. The step functions are due to the larger interval barometric pressure data used.
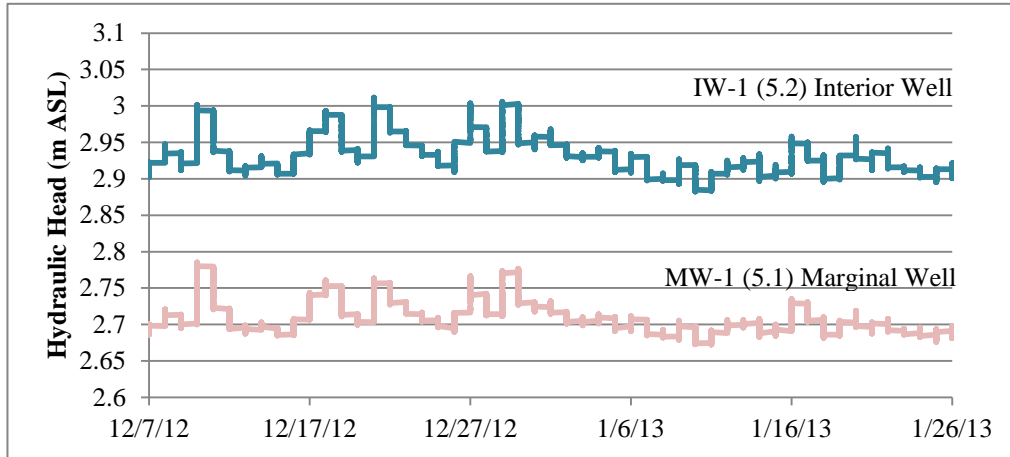
BIBLIOGRAPHY

Anderson, M. P. (2005), Heat as a ground water tracer, *Ground Water*, *43*(6), 951–968.

Baird, A. J. (1997), Field estimatation of macropore functioning and surface hydraulic conductivity in a fen peat, *Hydrol. Process.*, *11*, 287–295.

Beckwith, C. W., A. J. Baird, and a. L. Heathwaite (2003), Anisotropy and depth-related heterogeneity of hydraulic conductivity in a bog peat. II: modelling the effects on groundwater flow, *Hydrol. Process.*, *17*(1), 89–101, doi:10.1002/hyp.1116.

Beechie, T. J., D. a. Sear, J. D. Olden, G. R. Pess, J. M. Buffington, H. Moir, P. Roni, and M. M. Pollock (2010), Process-based Principles for Restoring River Ecosystems, *Bioscience*, *60*(3), 209–222, doi:10.1525/bio.2010.60.3.7.

Belyea, L. R., and R. S. Clymo (2001), Feedback control of the rate of peat formation., *Proc. R. Soc. London Biol.*, *268*, 1315–21, doi:10.1098/rspb.2001.1665.

Blasch, K. W., and J. R. Bryson (2007), Distinguishing sources of ground water recharge by using delta2H and delta18O., *Ground Water*, *45*(3), 294–308, doi:10.1111/j.1745-6584.2006.00289.x.

Blume, T., S. Krause, K. Meinikmann, and J. Lewandowski (2013), Upscaling lacustrine groundwater discharge rates by fiber-optic distributed temperature sensing, *Water Resour. Res.*, *49*(October 2012), 7929–7944, doi:10.1002/2012WR013215.

Boelter, D. H. (1968), Important Physical Properties of Peat Materials, *Proceeding 3rd Int. Peat Congr. Quebec, Canada*, 150–154.

Boelter, D. H. (1969), Physical properties of peats as related to degree of decomposition, *Soil Sci. Soc. Am. Proc.*, *33*, 606–609.

Boulton, A. J., S. Findlay, P. Marmonier, E. H. Stanley, and H. M. Valett (1998), The functional significance of the hyporheic zone in streams and rivers, *Annu. Rev. Ecol. Syst.*, *29*, 59–81.

Briggs, M. A., L. K. Lautz, and J. M. McKenzie (2012), A comparison of fibre-optic distributed temperature sensing to traditional methods of evaluating groundwater inflow to streams, *Hydrol. Process.*, *26*(9), 1277–1290, doi:10.1002/hyp.8200.

Briggs, M. A., E. B. Voytek, F. D. Day-Lewis, D. O. Rosenberry, and J. W. Lane (2013), Understanding water column and streambed thermal refugia for endangered mussels in the Delaware River., *Environ. Sci. Technol.*, *47*(20), 11423–31, doi:10.1021/es4018893.

Brunke, M., and T. Gonser (1997), The ecological significance of exchange processes between rivers and groundwater, *Freshw. Biol.*, *37*(1), 1–33.

Buffam, I., S. R. Carpenter, W. Yeck, P. C. Hanson, and M. G. Turner (2010), Filling holes in regional carbon budgets: Predicting peat depth in a north temperate lake district, *J. Geophys. Res.*, *115*(G1), G01005, doi:10.1029/2009JG001034.

Caissie, D. (2006), The thermal regime of rivers: a review, *Freshw. Biol.*, *51*(8), 1389–1406, doi:10.1111/j.1365-2427.2006.01597.x.

Campana, M. E., G. J. Wroblicky, J. A. Morrice, C. N. Dahm, H. M. Valett, and M. A. Baker (1994), Hyporheic zone mixing and residence time distributions, edited by Anonymous, *Geol. Soc. Am. 1994 Annu. Meet.*, *26*, 286.

Cardenas, M. B., and V. A. Zlotnik (2003), Three-dimensional model of modern channel bend deposits, *Water Resour. Res.*, *39*(6), 1141.

Chason, D. B., and D. I. Siegel (1986), Hydraulic conductivity and related physical properties of peat, Lost River peatland, northern Minnesota, *Soil Sci.*, *142*(2), 91–101.

Chen, X. H., J. X. Song, C. Cheng, D. M. Wang, and S. O. Lackey (2009), A new method for mapping variability in vertical seepage flux in streambeds, *Hydrogeol. J.*, *17*(3), 519–525, doi:Doi 10.1007/S10040-008-0384-0.

Cheng, X., and M. P. Anderson (1994), Simulating the influence of lake position on groundwater fluxes, *Water Resour. Res.*, *30*(7), 2041–2049.

Cherkauer, D. S., and P. F. McKereghan (1991), Ground-water discharge to lakes: focusing in embayments, *Ground Water*, *29*(1), 72–80.

Cherkauer, D. S., and J. P. Zager (1989), Groundwater interaction with a kettle-hole lake: relation of observations to digital simulations, *J. Hydrol.*, *109*(1-2), 167–184, doi:10.1016/0022-1694(89)90013-9.

Cirkel, D. G., J. M. Witte, and S. E. A. T. M. van der Zee (2010), Estimating seepage intensities from groundwater level time series by inverse modelling: A sensitivity analysis on wet meadow scenarios, *J. Hydrol.*, *385*(1-4), 132–142, doi:10.1016/j.jhydrol.2010.02.009.

Clymo, R. S. (1984), The Limits to Peat Bog Growth, *Philos. Trans. R. Soc. Lond. B. Biol. Sci.*, *303*(1117), 605–654.

Comas, X., L. Slater, and A. Reeve (2005), Stratigraphic controls on pool formation in a domed bog inferred from ground penetrating radar (GPR), *J. Hydrol.*, *315*(1-4), 40–51, doi:10.1016/j.jhydrol.2005.04.020.

Conant Jr., B. (2004), Delineating and Quantifying Ground Water Discharge Zones Using Steambed Temperatures, *Groundwater*, *42*(2), 243–257.

Constantz, J. (1998), Interaction between stream temperature, streamflow, and groundwater exchanges in Alpine streams, *Water Resour. Res.*, *34*(7), 1609–1615.

Constantz, J. (2008), Heat as a tracer to determine streambed water exchanges, *Water Resour. Res.*, *44*(W00D10), doi:10.1029/2008WR006996.

Cunliffe, A. M., A. J. Baird, and J. Holden (2013), Hydrological hotspots in blanket peatlands: Spatial variation in peat permeability around a natural soil pipe, *Water Resour. Res.*, *49*(9), 5342–5354, doi:10.1002/wrcr.20435.

Dahl, M., B. Nilsson, J. H. Langhoff, and J. C. Refsgaard (2007), Review of classification systems and new multi-scale typology of groundwater – surface water interaction, *J. Hydrol.*, *344*, 1–16, doi:10.1016/j.jhydrol.2007.06.027.

Davidson, E. A., and I. A. Janssens (2006), Temperature sensitivity of soil carbon decomposition and feedbacks to climate change., *Nature*, *440*(7081), 165–73, doi:10.1038/nature04514.

Deitchman, R., and S. P. Loheide II (2012), Sensitivity of Thermal Habitat of a Trout Stream to Potenial Climate Change, Wisconsin, United States, *J. Am. Water Resour. Assoc.*, *48*(6), 1091–1103, doi:10.1111⁄ j.1752-1688.2012.00673.x.

Deitchman, R. S., and S. P. Loheide (2009), Ground-based thermal imaging of groundwater flow processes at the seepage face, *Geophys. Res. Lett.*, *36*(14), L14401, doi:10.1029/2009GL038103.

Demars, B. O. L., J. Russell Manson, J. S. Ólafsson, G. M. Gíslason, R. Gudmundsdóttir, G. Woodward, J. Reiss, D. E. Pichler, J. J. Rasmussen, and N. Friberg (2011), Temperature and the metabolic balance of streams, *Freshw. Biol.*, *56*(6), 1106–1121, doi:10.1111/j.1365-2427.2010.02554.x.

DeMoranville, C. J. (2006), Cranberry Best Management Practice Adoption and Conservation Farm Planning in Massachusetts, *HorTechology*, *16*(September), 393–397.

Devito, K. J., J. M. Waddington, and B. A. Branfireun (1997), Flow reversals in peatlands influenced by local groundwater systems, *Hydrol. Process.*, *11*, 103–110.

Drexler, J. Z., B. L. Bedford, R. Scognamiglio, and D. I. Siegel (1999), Fine-scale characteristics of groundwater flow in a peatland, *Hydrol. Process.*, *13*, 1341–1359.

Dunne, T., and R. D. Black (1970), Partial area contributions to storm runoff in a small New England watershed, *Water Resour. Res.*, *6*(5), 1296–1311.

Ferland, M., P. T. Yves, C. Teodoru, and P. A. del Giorgio (2014), Linking organic carbon sedimentation, burial efficiency, and long-term accumulation in boreal lakes, *J. Geophys. Res. Biogeosciences*, *119*.

Fisher, E., G. A. Mcmechan, and A. P. Annan (1992), Acquisition and processing of wide-aperture ground-penetrating radar data, *Geophysics*, *57*(3), 495–504.

Fraser, C. J. D., N. T. Roulet, and M. Lafleur (2001), Groundwater flow patterns in a large peatland, *J. Hydrol.*, *246*(1-4), 142–154, doi:10.1016/S0022-1694(01)00362-6.

Freeze, A. R. (1988), Framework for assessing impacts on hydrology og nontidal wetlands, *Environ. Manage.*, *12*(5), 605–620.

Freeze, R. A., and P. A. Witherspoon (1967), Theoretical analysis of regional groundwater flow- 2. Effect of water-table configuration and subsurface permeability variation, *Water Resour. Res.*, *3*(2), 623–634.

Garrison, P. J., and S. A. Fitzgerald (2005), The role of shoreland development and commercial cranberry farming in a lake in Wisconsin , USA, *J. Paleolimnol.*, *33*(2), 169–188.

Genereux, D., and I. Bandopadhyay (2001), Numerical investigation of lake bed seepage patterns: effects of porous medium and lake properties, *J. Hydrol.*, *241*(3-4), 286–303, doi:10.1016/S0022-1694(00)00380-2.

Glaser, P. H., B. C. S. Hansen, D. I. Siegel, A. S. Reeve, and P. J. Morin (2004), Rates , pathways and drivers for peatland development in the Hudson Bay Lowlands , northern Ontario , Canada, , 1036–1053.

Gordon, R. P., L. K. Lautz, M. A. Briggs, and J. M. McKenzie (2012), Automated calculation of vertical pore-water flux from field temperature time series using the VFLUX method and computer program, *J. Hydrol.*, *420-421*, 142–158, doi:10.1016/j.jhydrol.2011.11.053.

Goto, S., M. Yamano, and M. Kinoshita (2005), Thermal response of sediment with vertical fluid flow to periodic temperature variation at the surface, *J. Geophys. Res. B Solid Earth*, *110*(1), B01106, doi:10.1029/2004JB003419.

Grand-Clement, E., K. Anderson, D. Smith, D. Luscombe, N. Gatis, M. Ross, and R. E. Brazier (2013), Evaluating ecosystem goods and services after restoration of marginal upland peatlands in South-West England, edited by S. Wan, *J. Appl. Ecol.*, *50*(2), 324–334, doi:10.1111/1365-2664.12039.

Grover, S. P. P., and J. a. Baldock (2013), The link between peat hydrology and decomposition: Beyond von Post, *J. Hydrol.*, *479*, 130–138, doi:10.1016/j.jhydrol.2012.11.049.

Hansen, B. P., and W. W. Lapham (1992), Geohydrology and simulated ground-water flow, plymouth-carver aquifer, southeastern Massachusetts, *United States Geol. Surv. Water Resour. Investig. Rep. 90-4204*.

Hatch, C. E., A. T. Fisher, J. S. Revenaugh, J. Constantz, and C. Ruehl (2006), Quantifying surface water-groundwater interactions using time series analysis of streambed thermal records: Method development, *Water Resour. Res.*, *42*(10).

Hill, A. R. (2012), The impact of pipe flow in riparian peat deposits on nitrate transport and removal, *Hydrol. Process.*, *26*(20), 3135–3146, doi:10.1002/hyp.8388.

Hoes, O. A. C., W. M. J. Luxemurg, M. C. Westhof, N. C. van de Giesen, and J. Selker (2009), Identifying seepage in ditches and canals in polders in the Netherlands by distributed temperature sensing, *Lowl. Technol. Int.*, *11*(2), 21–26.

Holden, J. (2004), Hydrological connectivity of soil pipes determined by ground-penetrating radar tracer detection, *Earth Surf. Process. Landforms*, *29*(4), 437–442, doi:10.1002/esp.1039.

Holden, J. (2005), Peatland hydrology and carbon release: why small-scale process matters., *Philos. Trans. A. Math. Phys. Eng. Sci.*, *363*(1837), 2891–913, doi:10.1098/rsta.2005.1671.

Holden, J., and T. P. Burt (2003), Hydraulic conductivity in upland blanket peat: measurement and variability, *Hydrol. Process.*, *17*(6), 1127–1237.

Holden, J., R. P. Smart, K. J. Dinsmore, a. J. Baird, M. F. Billett, P. J. Chapman, and R. Grayson (2012), Morphological change of natural pipe outlets in blanket peat, *Earth Surf. Process. Landforms*, *37*(1), 109–118, doi:10.1002/esp.2239.

Hunt, R. J., T. D. Bullen, D. P. Krabbenhoft, and C. Kendall (1998), Using stable isotopes of water and strontium to investigate the hydrology of a natural and constructed wetland, *Ground Water*, *36*(3), 434–443.

Ise, T., A. L. Dunn, S. C. Wofsy, and P. R. Moorcroft (2008), High sensitivity of peat decomposition to climate change through water-table feedback, *Nat. Geosci.*, *1*(11), 763–766, doi:10.1038/ngeo331.

Jones, J. a. a. (2010), Soil piping and catchment response, *Hydrol. Process.*, *24*(12), 1548–1566, doi:10.1002/hyp.7634.

Kellner, E., J. S. Price, and J. M. Waddington (2004), Pressure variations in peat as a result of gas bubble dynamics, *Hydrol. Process.*, *18*(13), 2599–2605, doi:10.1002/hyp.5650.

Kendall, C., and T. B. Coplen (2001), Distribution of oxygen-18 and deuterium in river waters across the United States, *Hydrol. Process.*, *15*(7), 1363–1393, doi:10.1002/hyp.217.

Kettridge, N., X. Comas, A. Baird, L. Slater, M. Strack, D. Thompson, H. Jol, and A. Binley (2008), Ecohydrologically important subsurface structures in peatlands revealed by ground-penetrating radar and complex conductivity surveys, *J. Geophys. Res.*, *113*, 1–15, doi:10.1029/2008JG000787.

Knight, R. (2001), Ground penetrating radar for environmental applications, *Annu. Rev. Earth Planet. Sci.*, *29*, 229–255.

Koteff, C., and F. Pessl (1981), Systematic ice retreat in New England, *United States Geol. Surv. Prof. Pap.*, *1179*.

Kruger, J., K. H. Kjaer, and A. Schomacker (2009), 7 Dead-Ice Environments: A Landsystems Model for a Debris-Charged, Stagnant Lowland Glacier Margin, Kötlujökull, *Dev. Quat. Sci.*, *13*, 105–126.

Labaugh, J. W., T. C. Winter, and D. O. Rosenberry (1998), Hydrologic Functions of Prairie Wetlands, *Gt. Plains Res.*, *8*, 17–37.

Lafleur, P. M., T. R. Moore, N. T. Roulet, and S. Frolking (2005), Ecosystem respiration in a cool Temperate bog depends on peat temperature but not water table, *Ecosystems*, *8*(6), 619–629, doi:10.1007/s10021-003-0131-2.

Larsen, L. G., J. W. Harvey, and J. P. Crimaldi (2007), A delicate balance: ecohydrological feedbacks governing landscape morphology in a lotic peatland, *Ecol. Monogr.*, *77*(4), 591–614.

Larson, G. J. (1982), Nonsynchronous retreat of ice lobes from southeastern Massachusetts, in *Late Wisconsinan Glaciation of New England*, pp. 101–114., Kendall/Hall Publishing Co, Dubuque, Iowa.

Leopold, M., and J. Volkel (2003), GPR images of periglacial slope deposits beneath peat bogs in the Central European Highlands, Germany, *Geol. Soc. London, Spec. Publ.*, *211*(1), 181–189, doi:10.1144/GSL.SP.2001.211.01.15.

Loheide, S. P., and S. M. Gorelick (2006), Quantifying stream-aquifer interactions through the analysis of remotely sensed thermographic profiles and in situ temperature histories, *Environ. Sci. Technol.*, *40*(10), 3336–3341.

Van Loon, A. H., P. P. Schot, J. Griffioen, M. F. P. Bierkens, O. Batelaan, and M. J. Wassen (2009), Throughflow as a determining factor for habitat contiguity in a near-natural fen, *J. Hydrol.*, *379*(1-2), 30–40, doi:10.1016/j.jhydrol.2009.09.041.

Lowry, C. S., J. F. Walker, R. J. Hunt, and M. P. Anderson (2007), Identifying spatial variability of groundwater discharge in a wetland stream using a distributed temperature sensor, *Water Resour. Res.*, *43*(10), 1–9, doi:10.1029/2007WR006145.

Lowry, C. S., D. Fratta, and M. P. Anderson (2009), Ground penetrating radar and spring formation in a groundwater dominated peat wetland, *J. Hydrol.*, *373*(1-2), 68–79, doi:10.1016/j.jhydrol.2009.04.023.

M.G.L (2000), *Wetlands Protection Act Regulations: 310 CMR 10.00*.

Masterson (2009), Hydrogeology and Simulation of Groundwater Flow in the Plymouth-Carver-Kingston-Duxbury Aquifer System , Southeastern Massachusetts Scientific Investigations Report 2009 – 5063,

McBride, M. S., and H. O. Pfannkuch (1975), Distribution of seepage within lakebeds, *US Geol. Surv. J. Res.*, *3*(5), 505–512.

McKenzie, J. M., D. I. Siegel, D. O. Rosenberry, P. H. Glaser, and C. I. Voss (2007), Heat transport in the Red Lake Bog , Glacial Lake Agassiz Peatlands, , *378*(December 2006), 369–378, doi:10.1002/hyp.

Newby, P. E., P. Killoran, M. R. Waldorf, B. N. Shuman, R. S. Webb, and T. Webb (2000), 14,000 Years of Sediment, Vegetation, and Water-Level Changes at the Makepeace Cedar Swamp, Southeastern Massachusetts, *Quat. Res.*, *53*(3), 352–368, doi:10.1006/qres.1999.2120.

Newby, P. E., J. P. Donnelly, B. N. Shuman, and D. MacDonald (2009), Evidence of centennial-scale drought from southeastern Massachusetts during the Pleistocene/Holocene transition, *Quat. Sci. Rev.*, *28*(17-18), 1675–1692, doi:10.1016/j.quascirev.2009.02.020.

Oakley, B. a., and J. C. Boothroyd (2012), Reconstructed topography of Southern New England prior to isostatic rebound with implications of total isostatic depression and relative sea level, *Quat. Res.*, *78*(1), 110–118, doi:10.1016/j.yqres.2012.03.002.

Parish, F., A. Sirin, D. Charman, H. Joosten, T. Minayeva, and M. Silvius (2008), *Assessment on Peatlands, Biodiversity and Climate Change: Main Report.*, edited by L. Stringer, Global Environment Centre, Kuala Lumpur & Wetlands International, Wageningen.

Parsekian, A. D., X. Comas, L. Slater, and P. H. Glaser (2011), Geophysical evidence for the lateral distribution of free phase gas at the peat basin scale in a large northern peatland, *J. Geophys. Res.*, *116*(G3), 1–14, doi:10.1029/2010JG001543.

Price, J. S., A. L. Heathwaite, and A. J. Baird (2003), Hydrological processes in abandoned and restored peatlands : An overview of management approaches, *Wetl. Ecol. Manag.*, *11*, 65–83.

Rau, G. C., M. S. Andersen, A. M. McCallum, H. Roshan, and R. I. Acworth (2014), Heat as a tracer to quantify water flow in near-surface sediments, *Earth-Science Rev.*, *129*, 40–58, doi:10.1016/j.earscirev.2013.10.015.

Reeve, a. ., D. . Siegel, and P. . Glaser (2000), Simulating vertical flow in large peatlands, *J. Hydrol.*, *227*(1-4), 207–217, doi:10.1016/S0022-1694(99)00183-3.

Reeve, A. S., R. Evensen, P. H. Glaser, D. I. Siegel, and D. Rosenberry (2006), Flow path oscillations in transient ground-water simulations of large peatland systems, *J. Hydrol.*, *316*(1-4), 313–324, doi:10.1016/j.jhydrol.2005.05.005.

Rennermalm, A. K., J. M. Nordbotten, and E. F. Wood (2010), Hydrologic variability and its influence on long-term peat dynamics, *Water Resour. Res.*, *46*(12), 1–18, doi:10.1029/2009WR008242.

Robinson, D. A., H. Abdu, S. B. Jones, M. Seyfried, I. Lebron, and R. Knight (2008), Eco-Geophysical Imaging of Watershed- Scale Soil Patterns Links with Plant Community Spatial Patterns, *Vadose Zo. J.*, *7*(4), 1132–1138.

Rosenberry, D. O., L. Toran, and J. E. Nyquist (2010), Effect of surficial disturbance on exchange between groundwater and surface water in nearshore margins, *Water Resour. Res.*, *46*(6), n/a–n/a, doi:10.1029/2009WR008755.

Rossi, P. M., P. Ala-aho, A.-K. Ronkanen, and B. Kløve (2012), Groundwater–surface water interaction between an esker aquifer and a drained fen, *J. Hydrol.*, *432-433*, 52–60, doi:10.1016/j.jhydrol.2012.02.026.

Rycroft, D. W., D. J. A. Williams, and H. A. P. Ingram (1975), The transmission of water through peat: I. Review, *Br. Ecol. Soc.*, *63*(2), 535–556.

Schmidt, C., B. Conant Jr., M. Bayer-Raich, and M. Schirmer (2007), Evaluation and field scale application of an analytical method to quantify groundwater discharge using mapped streambed temperatures, *J. Hydrol.*, *347*, 292–307.

Sebestyen, S. D., and R. L. Schneider (2001), Dynamic temporal patterns of nearshore seepage flux in a headwater Adirondack lake, *J. Hydrol.*, *247*, 137–150.

Sebestyen, S. D., and R. L. Schneider (2004), Seepage patterns, pore water, and aquatic plants: hydrological and biogeochemical relationships in lakes, *Biogeochemistry*, *68*(3), 383–409.

Selker, J. S. et al. (2006), Distributed fiber-optic temperature sensing for hydrologic systems, *Water Resour. Res.*, *42*(12), doi:doi:10.1029/2006WR005326.

Shuman, B., J. Bravo, J. Kaye, J. a Lynch, P. Newby, and T. Webb (2001), Late Quaternary Water-Level Variations and Vegetation History at Crooked Pond, Southeastern Massachusetts, *Quat. Res.*, *56*(3), 401–410, doi:10.1006/qres.2001.2273.

Siegel, D. I., A. S. Reeve, P. H. Glaser, and E. A. Romanowicz (1995), Climate-driven flushing of pore water in peatlands, *Nature*, *374*, 531–533.

Silliman, S. E., J. Ramirez, and R. L. Mccabe (1995), Quantifying Downflow through Creek Sediments Using Temperature Time-Series - One-Dimensional Solution Incorporating Measured Surface-Temperature, *J. Hydrol.*, *167*(1-4), 99–119.

Slater, L. D., and A. Reeve (2002), Case History Investigating peatland stratigraphy and hydrogeology using integrated electrical geophysics, *Geophysics*, *67*(2), 365–378.

Smart, R. P., J. Holden, K. J. Dinsmore, A. J. Baird, M. F. Billett, P. J. Chapman, and R. Grayson (2012), The dynamics of natural pipe hydrological behaviour in blanket peat, , doi:10.1002/hyp.

Sophocleous, M. (2002), Interactions between groundwater and surface water: the state of the science, *Hydrogeol. J.*, *10*(1), 52–67.

Stallman, R. W. (1965), Steady one-dimensional fluid flow in a semi-infinite porous medium with sinusoidal surface temperature, *J. Geophys. Res.*, *70*(12), 2821–2827, doi:Cited By (since 1996) 106 Export Date 4 April 2012.

Stone, B. D., J. R. Stone, M. L. Digiacomo-cohen, and K. A. Kincare (2011), , Surficial geologic map of the Norton-Manomet-Westport-Sconticut Neck 23-quadrangle area in southeast Massachusetts, *United States Geol. Surv. Open File Rep. 2006-1260-F*, *21 sheets*(scale 1:24000), 22.

Stonestrom, D. A., and J. Constantz (2004), *Heat as a Tool for Studying the Movement of Ground Water Near Streams*, U. S. Geological Survey Circular 1260.

Swain, M., M. Swain, M. Lohmann, and E. Swain (2012), Experimental determination of soil heat storage for the simulation of heat transport in a coastal wetland, *J. Hydrol.*, *422-423*, 53–62, doi:10.1016/j.jhydrol.2011.12.036.

Taniguchi, M. (2002), Estimations of the past groundwater recharge rate from deep borehole temperature data, *Catena*, *48*, 39–51.

Topp, G. C., J. L. Davis, and A. P. Annan (1980), Electromagnetic Determination of Soil Water Content:, *Water Resour. Res.*, *16*(3), 574–582.

Turcotte, D. L., and G. Schubert (1982), Geodynamics: Applications of Continuum Physics to Geological Problems, *John Wiley Sons, New York*.

Tyler, S. W., J. S. Selker, M. B. Hausner, C. E. Hatch, T. Torgersen, C. E. Thodal, and S. G. Schladow (2009), Environmental temperature sensing using Raman spectra DTS fiber-optic methods, *Water Resour. Res.*, *45*, doi:doi:10.1029/2008WR007052.

Vandenbohede, a., P. G. B. de Louw, and P. J. Doornenbal (2014), Characterizing preferential groundwater discharge through boils using temperature, *J. Hydrol.*, *510*, 372–384, doi:10.1016/j.jhydrol.2014.01.006.

Verberk, W. C. E. P., D. T. Bilton, P. Calosi, and J. I. Spicer (2011), Oxygen supply in aquatic ectotherms: Partial pressure and solubility together explain biodiversity and size patterns, *Ecology*, *92*(8), 1565–1572.

Wallage, Z. E., and J. Holden (2011), Near-surface macropore flow and saturated hydraulic conductivity in drained and restored blanket peatlands, *Soil Use Manag.*, *27*(2), 247–254, doi:10.1111/j.1475-2743.2011.00336.x.

Watters, J. R., and E. H. Stanley (2007), Stream channels in peatlands: The role of biological processes in controlling channel form, *Geomorphology*, *89*(1-2), 97–110, doi:10.1016/j.geomorph.2006.07.015.

Winter, T. C. (1976), Effects of water-table configuration on seepage through lakebeds, *Limnol. Oceanogr.*, *26*(5), 925–934.

Winter, T. C. (2001), The concept of hydrologic landscapes, *J. Am. Water Resour. Assoc.*, *37*(2), 335–349.

Winter, T. C., and J. W. Labaugh (2003), Hydrologic Considerations in Defining Isolated Wetlands, *Wetlands*, *23*(3), 532–540.

Worrall, F., P. Chapman, J. Holden, C. Evans, R. Artz, P. Smith, and R. Grayson (2010), Peatlands and Climate Change: Scientific Review, *IUCN UK Peatl. Program.*, (December), 1–15.